BrGDGT-based palaeothermometer in drylands: the necessity to constrain aridity and salinity as confounding factors to ensure the robustness of calibrations.

Lucas Dugerdil[1,2], Sébastien Joannin[1], Odile Peyron[1], Shafag Bayramova[3], Xiaozhong Huang[4,5],
Fahu Chen[4,6,7], Dilfuza Egamberdieva[8,9], Jakhongir Alimov[10,11], Bazartseren Boldgiv[12],
Amy Cromartie[13,1], Juzhi Hou[6,7], Lilit Sahakyan[14], Khachatur Meliksetian[14], Salomé Ansanay-Alex[2],
Rafig Safarov[15], Imran Muradi[15], Shabnam Isayeva[16], Shehla Mirzayeva[16], Elshan Abdullayev[17,18],
Sayyara Ibadullayeva[16], Parvana Garakhani[16], and Guillemette Ménot[2]

[1]ISEM, Univ Montpellier, CNRS, IRD, Montpellier, France
[2]ENS Lyon, UCBL, CNRS, UMR 5276 LGL-TPE, Lyon, France
[3]Institute of Geology and Geophysics, Department of modern geodynamics and space geodesy, Azerbaijan
[4]Key Laboratory of Western China's Environmental Systems (Ministry of Education), College of Earth and Environmental Sciences, Lanzhou University, Lanzhou, China
[5]Yunnan Key Laboratory of Plateau Geographical Processes and Environmental Changes, Faculty of Geography, Yunnan Normal University, Kunming 650500, China
[6]Alpine Paleoecology and Human Adaptation Group, State Key Laboratory of Tibetan Plateau Earth System, Resources and Environment, Institute of Tibetan Plateau Research, Chinese Academy of Sciences, Beijing, China
[7]College of Resources and Environment, University of Chinese Academy of Sciences, Beijing, China
[8]Institute of Fundamental and Applied Research, National Research Univ. (TIIAME), Tashkent 100000, Uzbekistan
[9]Leibniz Centre for Agricultural Landscape Research (ZALF), 15374 Müncheberg, Germany
[10]International Agriculture University, Kibray district, 100164, Tashkent, Uzbekistan
[11]Faculty of Biology, National University of Uzbekistan, 100174, Tashkent, Uzbekistan
[12]Ecology Group, Department of Biology, School of Arts and Sciences, National University of Mongolia, Ulaanbaatar 14201, Mongolia
[13]Université Côte d'Azur, CNRS, CEPAM, UMR 7264, 06300, Nice, France
[14]National Academy of Sciences, Institute of Geological Sciences of Armenia, ave. M. Baghramyan 24a, Yerevan 0019, Armenia
[15]Institute of Geology and Geophysics, Science and Education Ministry of Azerbaijan Republic, AZ1073, Baku, Azerbaijan
[16]Institute of Botany, Azerbaijan National Academy of Sciences, Baku, Azerbaijan
[17]Institute of Geography and Geology, University of Greifswald, Friedrich-Ludwig-Jahn Strasse 17A, D-17487 Greifswald, Germany
[18]Department of Life Sciences, Khazar University, 41 Mahsati Str., AZ1096 Baku, Azerbaijan

Correspondence: Lucas Dugerdil (lucas.dugerdil@ens-lyon.fr) and Guillemette Ménot (guillemette.menot@ens-lyon.fr)

Abstract. Past temperature reconstructions offer valuable insights into the impact of climate change on the global climate-human-vegetation system. Branched glycerol dialkyl glycerol tetraethers (brGDGTs) are recognized as effective temperature proxies, particularly in lakes and peatlands, where they are well preserved. However, their reliability as palaeothermometers can be compromised by factors beyond air temperature, especially in drylands. This study ~~introduces the~~ further explores the recently compiled Arid Central Asian (ACA) brGDGT surface Data Base, a regional dataset consisting of ~~162 new~~ 761 surface samples from the drylands of ACA~~, in addition to 599 previously published samples~~. The distribution of brGDGTs in relation to

climate and environmental variables was analysed to explore their potential as reliable temperature proxies, mainly focusing on brGDGTs methylation (MBT), cyclisation (CBT), and isomer (IR) indices. The brGDGT-based palaeothermometer is a promising tool for understanding past climates, but our comparison between an ACA-centred database and a worldwide continental surface sample database reveals several challenges. Drylands exhibit extreme climate and soil/lacustrine properties, amplifying the impact of confounding factors on brGDGT-based relationships with mean annual air temperature. Salinity emerges as the dominant factor influencing brGDGT variance, followed by sample type, pH, and aridity, all of which contribute significantly. These factors interact in complex ways, with the salinity effect varying between soil and lacustrine deposits. For sample physicochemical conditions, the IR'_{6+7Me} index is best for salinity, and IR_{6Me} is most suitable for pH reconstruction. Despite this, the MBT'_{5Me}-temperature relationship is limited in ACA, particularly for lacustrine samples, and MBT'_{6Me} does not offer a better solution under hyper- to semi-arid conditions. Sub-calibrating models for specific environmental conditions such as salinity and aridity improves the accuracy of temperature reconstructions. Furthermore, the difference between MBT'_{5Me} and MBT'_{6Me} provides a promising proxy to assess aridity. Although the brGDGT signal in drylands is influenced by multiple ~~confounding~~ controlling factors, it remains a valuable tool for understanding past climate and environmental conditions, especially when accounting for the complex interactions between these factors based on each study's unique physicochemical and bioclimatic context. Further research, incorporating a broader range of surface samples alongside comprehensive soil and climate data, holds the potential to enhance the accuracy of brGDGT-based climate reconstructions.

1   Introduction

Given the uncertain implications of the anthropogenic climate change on the environment, hydrology and human society, reconstructions of the past climate temperatures provide a comprehensive perspective on the impact of climate change on the climate-human-vegetation system (Tierney et al., 2020). Branched glycerol dialkyl glycerol tetraethers (brGDGT) are ~~new~~ promising temperature proxies that have been used on continental archives (Weijers et al., 2007; Peterse et al., 2012; De Jonge et al., 2014; Dearing Crampton-Flood et al., 2020; Raberg et al., 2021), especially since these lipid compounds produced from bacterial membranes are ubiquitous (Raberg et al., 2022b), well preserved on past archives ~~of~~ retrieved from lakes (Dang et al., 2016b; Wang et al., 2021; So et al., 2023) and peatlands (Naafs et al., 2017a, b; d'Oliveira et al., 2023). ~~From laboratory experiments (Halamka et al., 2023), simulations (Naafs et al., 2021), but especially from soil surface samples (De Jonge et al., 2014; Dearing Crampton-Flood et al., 2020) or lake surface sediments (Sun et al., 2011), the~~ The number of methyl groups on the aliphatic chain of brGDGT changes with ~~air~~ ambient temperature, as shown by Weijers et al. (2007) and De Jonge et al. (2014), permitting their use as past temperature proxy. The relationship between the temperature and the brGDGT degree of methylation is clear and linear. ~~The diverse~~, from both soil surface samples (De Jonge et al., 2014; Dearing Crampton-F and lacustrine surface sediments (Sun et al., 2011). Same relationship is observed from laboratory experiments and simulations (Naafs et al., 2021; Halamka et al., 2023). The applications of brGDGT-based palaeothermometers ~~cover a wide range of~~ span ~~many~~ environments and archives~~: from tropical (Pérez-Angel et al., 2020; Häggi et al., 2023) to arctic lakes (Raberg et al., 2022a); from acid (Dang et al., 2016a)~~, including tropical to Arctic lakes (Pérez-Angel et al., 2020; Häggi et al., 2023; Raberg et al., 2022a)

40 ~~, acidic to~~ alkaline lakes ~~(Yang et al., 2014; Dang et al., 2016a); and also from loess-palaeosol sequences (Lin et al., 2024), freshwater (Dugerdil et al., 2021b; Robles et al., 2022)~~ (Dang et al., 2016a; Yang et al., 2014), freshwater to saline lakes ~~(Wang et al., 2021)~~ (Dugerdil et al., 2021b; Wang et al., 2021; Robles et al., 2022; So et al., 2023), and sediment from loess–palaeosols sequences (Lin et al., 2024). However, the change in the relative proportion of brGDGTs does not depend solely on the air temperature, which can significantly undermine the reliability of the palaeothermometer (e.g., pH, precipitation; Duan et al., 2020; Chen et al., 2021; Du

45 .

The influence of pH on brGDGT distribution was initially identified and thoroughly constrained (Weijers et al., 2007). pH primarily influences the relative number of 5- and 6-methyl isomers and the number of cyclisations along the aliphatic chain, while temperature affects the number of methylations (e.g., higher amount of tetramethylated compounds over warm environment, Sun et al., 2011; Peterse et al., 2012; Dang et al., 2016a; Raberg et al., 2022b). De Jonge et al. (2014) present the

50 application of the index of methylation of branched tetraethers ($\mathrm{MBT}'_{5\mathrm{Me}}$) index associated with mean annual air temperature (MAAT), the isomer ratio (IR), and the cyclisation of branched tetraethers (~~CBT'~~$\mathrm{CBT}_{5\mathrm{Me}}$) indices related to pH. These two important indices are now widely adopted to calibrate the reconstruction of pH and MAAT in the past by linear relationships. The sample type, including peat, soil, river, marine, loess, and lacustrine samples, influences the brGDGT-temperature relationship (Loomis et al., 2011; Martínez-Sosa et al., 2023). At the global scale, various specific calibrations between $\mathrm{MBT}'_{5\mathrm{Me}}$ and

55 MAAT have been suggested for soil (De Jonge et al., 2014; Chen et al., 2021), peat (Naafs et al., 2017b), and lacustrine samples (Sun et al., 2011; Zhao et al., 2021). The influence of the calibration database size and the biogeographical characteristics of brGDGT distribution has also been examined (Dugerdil et al., 2021a), and several local or regional calibrations allow for more accurate MAAT reconstructions in past archives (Chen et al., 2021). Subsequently, an increased number of confounding factors have been identified, e.g., soil moisture (Dang et al., 2016b) and sample type (e.g., soil or lacustrine; Martin et al.,

60 2019; Martínez-Sosa et al., 2021; Martínez-Sosa et al., 2023); temperature seasonality (Deng et al., 2016; Dearing Crampton-Flood et al., 2020), or vegetation (Häggi et al., 2023). ~~Thus~~For instance, the lacustrine samples have lower abundances of ~~pentamethyls~~ pentamethylated brGDGTs than soil samples (De Jonge et al., 2014; Martin et al., 2019; Raberg et al., 2022b), while peat samples are dominated by ~~tetramethyls~~ tetramethylated brGDGTs (Naafs et al., 2017a). The relationship between brGDGTs and MAAT may exhibit a bias toward the summer temperatures, particularly in soils and lakes that experience a

65 long frost period (Deng et al., 2016; Dearing Crampton-Flood et al., 2020). Vegetation influences the distribution of brGDGTs, likely due to the higher soil organic content found in vegetated soils compared to bare soils (Liang et al., 2019). This leads to a ~~differential~~ different temperature relationship between brGDGTs in soils and MAAT across different vegetation communities (Häggi et al., 2023).

~~Confounding~~ The interaction across controlling factors introduce various biases depending on geographic and climatic con-

70 texts. While they have been extensively studied in tropical regions and high-latitude or high-altitude environments (Pérez-Angel et al., 2020; Raberg et al., 2021; Zhao et al., 2021; Häggi et al., 2023), they remain poorly constrained in semi-arid to hyper-arid areas (Yang et al., 2014; Duan et al., 2020; Guo et al., 2021). In drylands, limited and erratic precipitation is the primary water input, critically influencing soil moisture. This persistent water deficit intensifies aridity, which is defined by the imbalance between precipitation and evapotranspiration (Trabucco and Zomer, 2018). Such bioclimatic stress affects soil chemistry, often
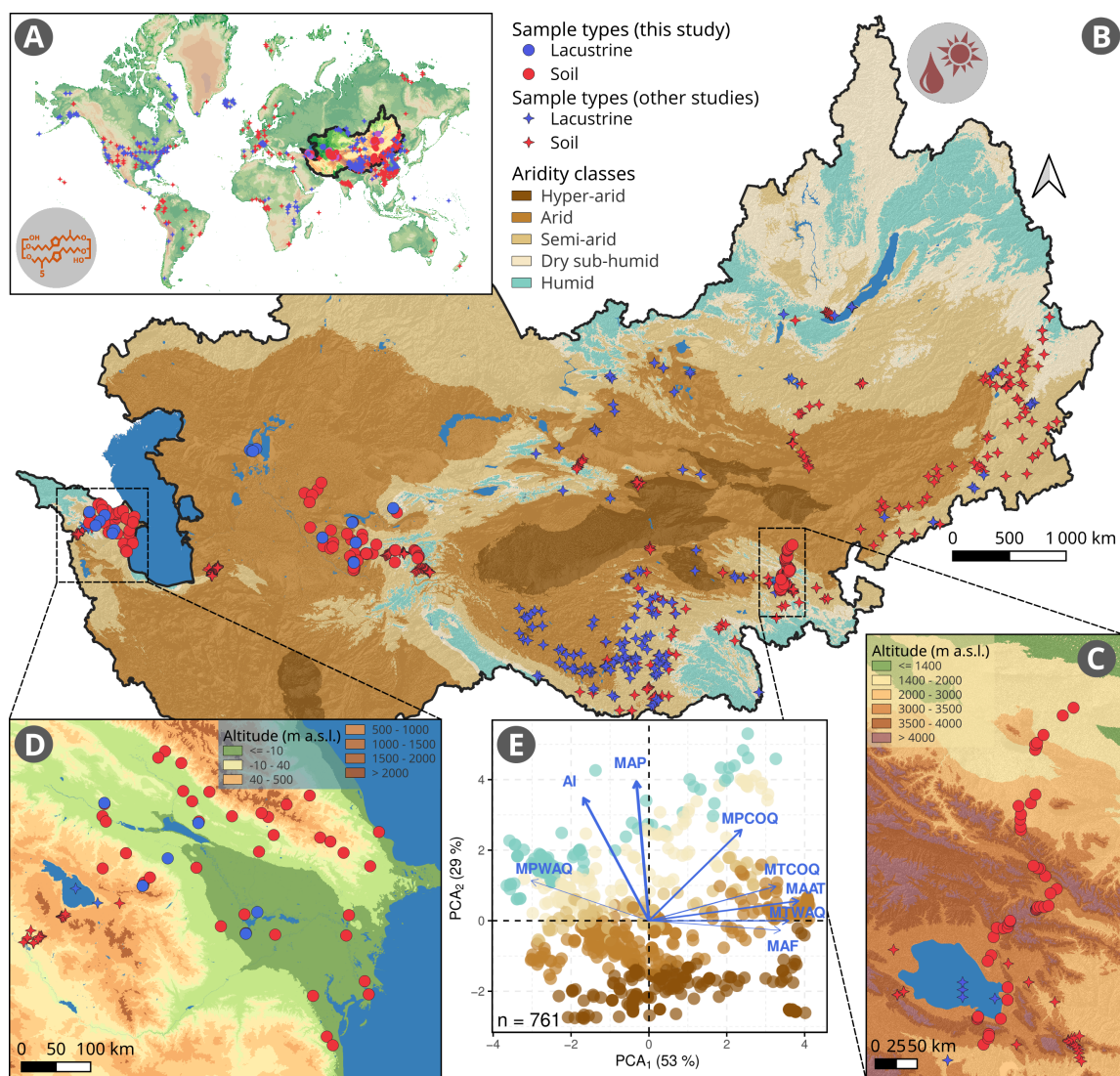
Figure 1. Distribution map of the global surface samples presented in this study (WDB, **A**) followed by the extent of the Arid Central Asian brGDGT surface Data Base (ACADB, **B**) and local focus on (**C**) Qilian Shan and (**D**) Caucasus surface samples. (**E**) distribution of brGDGT sampling sites in the ACA bioclimate space. The elevation map comes from SRTM Digital Elevation Model version 4.1 (Jarvis et al., 2008), the Aridity Index from CGIAR (Trabucco and Zomer, 2018) and the extracted climate parameters from worldclim2.1 (Fick and Hijmans, 2017) with mean air temperature of Months Above Freezing, Mean Annual Air Temperature, Mean Annual Precipitation, Mean Temperature/Precipitation of the Cold and Warm Quarters.

reducing leaching and causing the accumulation of base cations (e.g., calcium, magnesium), which contributes to alkaline soils with low organic matter content (Muhammad et al., 2008). Coarse-textured, well-drained soils are also common, increasing the occurrence of gypsum or saline profiles (Plaza et al., 2018). Additionally, sparse vegetation - further stressed by intense

grazing pressure - exacerbates land degradation (Maestre et al., 2022). The combined effects of aridity and overgrazing increase soil vulnerability to erosion, reinforcing a cycle of organic matter depletion, nutrient loss, and alkaline soil dominance

80 (Moreno-Jiménez et al., 2019). As a result, brGDGT-based reconstructions in drylands are especially prone to biases driven by bare soil conditions, aridity, and soil chemistry impacts on bacterial communities.

Primarily arid soils, characterized as soils receiving less than 500 $\mathrm{mm.yr^{-1}}$ (Peterse et al., 2012; Yang et al., 2014; Guo et al., 2021), present higher brGDGT variability and specific isomer distribution (Guo et al., 2021). The comparison of soil samples from drylands indicates a dissimilarity to global brGDGT databases (Yang et al., 2014; Dearing Crampton-Flood et al.,

85 2020; Véquaud et al., 2022). The main difference is the higher frequency of 6- compared to 5-methyl compounds (Duan et al., 2020). This distinct methylation process may explain the reduced statistical strength for brGDGT-temperature calibration under arid conditions (Peterse et al., 2012; Wang et al., 2019). Moreover, the temperature control over tetramethylated compounds may be related to 5- or 6-methyl assemblages in diverse contexts, likely due to specific bacterial communities, mitigating the reliability of $\mathrm{MBT'_{5Me}}$-based temperature reconstruction (Wang et al., 2024). Additionally, Duan et al. (2022) report the

90 influence of pH and, in particular, alkalinity on the distribution of brGDGTs in dry soils. A few recent studies have reported the impact of salinity on brGDGTs (Wang et al., 2021; Raberg et al., 2021; Kou et al., 2022; So et al., 2023). Salinity is ~~expected~~ thought to influence the relative number of 5-, 6- and 7-methyl isomers (Wang et al., 2021). This effect impacts the $\mathrm{MBT'_{5Me}}$- and $\mathrm{MBT'_{6Me}}$-based temperature reconstructions (Kou et al., 2022; So et al., 2023). Although several palaeosalinity proxies have been proposed to address these biases, significant work remains to be undertaken, for instance, on the precise

95 ionic composition of soil (Chen et al., 2022; De Jonge et al., 2024a). Among the possible solutions to reduce these biases, the brGDGT-temperature relationship independent of these two indexes includes Multiple linear Regressions (MR; De Jonge et al., 2014; Raberg et al., 2021), Bayesian calibrations (Dearing Crampton-Flood et al., 2020), and machine learning approaches (Véquaud et al., 2022). However, the coupled effects of aridity, pH and salinity on soil, loess, and lacustrine archives can significantly alter the interpretations of brGDGT-based climate reconstructions in the ACA region (Lin et al., 2024).

100 This study ~~presents~~ relies on the first regional database of surface brGDGT samples for drylands, aiming to identify the key climate and environmental parameters influencing their distribution. This dataset, referred to as the Arid Central Asian brGDGT Surface Database (ACADB), includes brGDGT assemblages from various sites across the region, totalling 761 ~~sites. It includes~~ samples. This dataset was compiled by Dugerdil et al. (2025a) to train machine learning models for climate reconstructions. The dataset combines 162 new ~~sites collected from four countries in ACA and aggregated~~ samples collected across four

105 ACA countries with 599 previously published ~~samples from ACA~~ records (Fig. 1). ~~These modern samples are analysed in relation to~~ In Dugerdil et al. (2025a), machine learning calibrations outperformed traditional linear models, suggesting that confounding factors weaken linear brGDGT–temperature relationships. The present study tests this hypothesis by analysing modern brGDGT distributions against key climate parameters, ~~mainly~~ including aridity, temperature ~~, and~~ (both Mean Annual Air Temperature, MAAT, and the seasonal mean temperature of Months Above Freezing, MAF), and precipitation, as well

110 as chemical characteristics such as pH, salinity, and sample type (soil or lacustrine). The results are then compared with the global Worldwide brGDGT Surface Database (WDB; modified from Raberg et al., 2022a) to assess whether similar brGDGT

patterns are observed at both regional and global scales. The methodological approach is synthesized in Fig. 2. Following this workflow, this study raises the following questions:

1. Which confounding factor - pH, aridity, salinity, or sample type - has the most significant impact on brGDGT-temperature calibrations in drylands?

2. Are the MBT'_{5Me} and MBT'_{6Me} reliable for reconstructing past temperature in this context?

3. Can we apply aridity- or salinity-related indices to soil and lacustrine samples similarly, or do we need to develop new indices or calibrations to track these ~~confounding~~ controlling factors?

2 Materials and Methods

2.1 Study sites

This study pools ~~new~~ samples from four different ACA countries: Azerbaijan, China (from the Qaidam Basin to the Qilian Mountains), Tajikistan, and Uzbekistan for a total of 162 samples ~~(Fig. 2, step 1).~~ (Fig. 2, step 1 and Dugerdil et al., 2025a). No data has previously been ~~published~~ analysed for Azerbaijan and Uzbekistan. All site coordinates and geographic features are presented in Fig. 1 and in Table S.1. From the Caucasus, 48 ~~new~~ surface sites are presented from Azerbaijan. ~~The data location was randomly selected and~~ Prior to the field campaign, sample locations were defined using a randomized selection procedure within a GIS framework to enhance the bioclimatic and ecological representativeness of the dataset (Bunting et al., 2013). Thus, the dataset covers all of Azerbaijan, from the Great Caucasus to the Hyrcanian forest in the Talish Range, through the Lesser Caucasus Range, the Mil Plain, and the Kura Valley (Fig. 1B). In China, an altitudinal/latitudinal gradient from the Qinghai Plateau to the southern part of the Gobi Desert, through the Qilian Shan Range, presents 48 new surface samples (Fig. 1C). For the Tajikistan-Uzbekistan database (TUSDB), the 66 sites come from the Aral Sea basin to the high Pamir-Alai Range. The site location and climatic presentation of the TUSDB is also available in Dugerdil et al. (2025b). The summarized information of each dataset is gathered in Table 1.

Temperature and precipitation maps for the ACA are provided in Fig. 2 from Dugerdil et al. (2025a), and additional ACA climographs are shown in Fig. S.1. MAAT for the ACADB has an average value of 3.7 ± 3.2 °C and it is balanced between warm/mild environments (MAAT > 10 °C), mainly on the western part of the ACA covering Caucasus (Armenia, Azerbaijan) and Middle Asia (Uzbekistan and Tajikistan), and colder continental environments (MAAT < 3 °C) located in Central Asia (i.e., the southern part of Siberia, the Mongolian plateau, and the Tibetan-Qinghai plateau in China, Table 1). On the opposite, the MAF is more homogeneous with low MAF in China (MAF = 7.5 ± 2.7 °C) and high MAF in Tajikistan and Uzbekistan (13 ± 2.5 °C). This is due to the higher seasonality in continental Central Asia than in the Caucasus and Middle Asia (Fig. S.1). Similarly, Mean Annual Precipitation is spatially homogeneous, with consistent low values of 410 ± 140 mm.yr^{-1}. However, the seasonal precipitation pattern varies greatly across ACA. In the western region - including the Caucasus, Iran, and Middle Asia - winter dominates, with up to 65% of annual rainfall occurring during this season. In contrast, the eastern region, encompassing the Central Asian plateaus and southern Siberia, receives up to 87% of its precipitation in summer (Chen et al., 2024).

Table 1. BrGDGT dataset compiled in the Arid Central Asian Database (ACADB) and Worldwide Database (WDB) with their associated average climate parameters, data description (covered countries, dataset size, and site elevation), and original publications. New data ~~published from Dugerdil et al. (2025a),~~ analysed in ~~this~~ the present study are highlighted by a ***** for a total sum of 162 surface samples.

Countries	N	Average bioclimate parameters[a]				Altitude	Original publication
		MAAT (°C)	MAF (°C)	MAP (mm.yr^{-1})	AI	(m a.s.l.)	
ACA lakes	52	1.8 ± 3.4	12 ± 2.7	260 ± 120	2500 ± 1500	1200 ± 890	Wang et al. (2021)
Armenia	22	6.8 ± 3.4	12 ± 2.4	420 ± 110	3600 ± 1300	1900 ± 610	Cromartie et al. (2025)
Azerbaijan	**48***	12 ± 3.3	13 ± 1.8	510 ± 160	4200 ± 1600	560 ± 630	This study; Dugerdil et al. (2025a)
China	120	3.7 ± 6	12 ± 4.7	290 ± 170	2800 ± 2000	1600 ± 1300	Wang et al. (2020); Wang and Liu (2021); Zang et al. (2018); Dang et al. (2018)
China, Inner Mong.	43	1.3 ± 2.4	12 ± 1.1	280 ± 51	2400 ± 730	930 ± 310	Guo et al. (2021); Li et al. (2017)
China, Qinghai	**48***	-0.012 ± 3.2	7.5 ± 2.7	410 ± 98	4400 ± 1900	3200 ± 680	This study; Dugerdil et al. (2025a)
China, Tian Shan	18	-2.1 ± 4.6	8.9 ± 5.5	280 ± 76	3900 ± 2400	2200 ± 760	Duan et al. (2020)
China, Tibet	129	-1.5 ± 3	6.1 ± 1.4	240 ± 130	2200 ± 1200	4600 ± 240	Kou et al. (2022)
Global BayMBT Soils	15	-1 ± 2.5	8.8 ± 2.8	330 ± 110	3000 ± 1200	2800 ± 1800	Dearing Crampton-Flood et al. (2020)
Global soils	48	0.46 ± 3.6	7.8 ± 3.3	380 ± 76	3400 ± 1000	3600 ± 1500	Naafs et al. (2017a)
Mongolia	31	1.1 ± 2.4	12 ± 2.2	230 ± 78	2200 ± 1000	1500 ± 220	Dugerdil et al. (2021a)
Northern Iran	48	17 ± 0.84	17 ± 0.6	330 ± 15	1900 ± 110	270 ± 140	Duan et al. (2022)
Russia, Baikal	20	-0.21 ± 1.8	9.3 ± 0.9	430 ± 92	5400 ± 1000	530 ± 97	De Jonge et al. (2015); Khodzher et al. (2017); Dugerdil et al. (2021a); Wang et al. (2021)
Tajikistan	(53+**12***)	4.7 ± 4.6	11 ± 2.4	470 ± 260	3700 ± 1800	2600 ± 880	This study; Chen et al. (2021); Dugerdil et al. (2025a)
Uzbekistan	**54***	12 ± 3.3	14 ± 2.2	360 ± 210	2300 ± 1600	1000 ± 760	This study; Dugerdil et al. (2025a)
Total ACA	**761**	**3.7 ± 3.2**	**11 ± 2.4**	**350 ± 120**	**3200 ± 1400**	**1900 ± 720**	
World DB	**2709**	**12 ± 8.8**	**14 ± 6.6**	**1200 ± 640**	**11000 ± 6400**	**730 ± 890**	Raberg et al. (2022b)[b]

[a] Bioclimate parameters refer to Mean Annual Air Temperature (MAAT), mean air temperature of Months Above Freezing (MAF), Mean Annual Precipitation (MAP), and Aridity Index (AI). Data were extracted from `worldclim2.1` (Fick and Hijmans, 2017) and `CGIAR` (Trabucco and Zomer, 2018). [b] for all original publications compiled in Raberg et al. (2022b), please report to Table S.2.

This spatial diversity within the ACA likely induces important heterogeneity in the bacterial growth season (i.e., fall and spring in western ACA, summer in eastern ACA, Fig. S.1). In arid environments, brGDGT production may be influenced by water availability, potentially increasing during the rainy season. This could bias reconstructed temperatures toward rainy-season conditions (De Jonge et al., 2014). The ACA altitudinal gradient reached by the database covers -28 to 4038 m a.s.l. with an average value of about 1600 m a.s.l.

2.2 Environmental parameters

The ~~new~~ newly described samples from this study (n = 162) are grouped into two main sample types: soil (n = 143) and lacustrine (n = 19) samples. Here, *soil* means a sample collected on the surface from several subsamples collected within one m^2 area and from the upper five cm part of the soil layer. *Lacustrine* corresponds to samples from lake sediment ~~core-tops~~ core

tops or surface sediments. The majority of these lakes are in arid environments, seasonally dried, and associated with temporary ponds. For lacustrine samples, one cm^3 of the upper parts of several ~~top cores~~ core tops were sampled using a die-cut or from the upper five cm of the surface sediment. For more details on the sample type description, please refer to Dugerdil et al. (2021a). For the sampling method of the already published samples, refer to the original publications (Duan et al., 2020, 2022; Wang et al., 2021; Raberg et al., 2022b; Kou et al., 2022). In total, the ACADB is composed of 560 soil and 201 lacustrine samples.

Following the field campaign, samples were stored at freezing temperature and analysed at the earliest opportunity to minimise post-sampling alterations of brGDGT distributions and chemical properties that may arise from ongoing microbial metabolic activity. The chemical characteristics of the ACA surface samples include pH and Electro-Conductivity (EC, Fig. 2, step 2), both measured *ex-situ* in the laboratory, even for lacustrine samples. These measurements were performed in the Montpellier laboratory using a HANNA Instruments HI991301 after a two-points calibration for pH and a single calibration for EC (mS/cm). Salinity, in terms of Total Dissolved Solids (TDS), was extrapolated from the EC following Rusydi (2018), Eq. (1):

$$TDS = \alpha \times EC_T \times 10^3 \tag{1}$$

with TDS in mg/L extrapolated from the EC at ambient temperature (EC_T) in mS/cm corrected by a conversion factor $\alpha \in [0.5; 0; 8]$ depending on the sample type (Rusydi, 2018). In Tibetan Plateau, the selected values are 0.65 or 0.8 (values from Supplementary Materials in Kou et al., 2022). Due to the wide range of salinity values among samples, it is mainly expressed in $\log_{10}$ (Kou et al., 2022). For new samples, a α of 0.65 was applied in this study to convert EC in TDS (i.e., in salinity). The EC_T is temperature compensated with Eq. (2):

$$EC_T = EC_{25\,°C} \times \beta T \tag{2}$$

where $\beta = 1.9\%$ is the temperature correction coefficient, T is the temperature in degrees Celsius, and $EC_{25,°C}$ is the electrical conductivity standardized to 25 °C, as conventionally defined. For the salinity of samples published in Wang et al. (2021) and Kou et al. (2022), please refer to the method section of both publications. The TDS values were used to provide four salinity classes (fresh, hyposaline, saline and hypersaline). The cut-off values were derived from Rusydi (2018) and refine for the ACADB using a sensitivity analysis (Table S.3). In the ACADB, salinity values are available for 113 soil and 67 lacustrine samples.

Since only a few weather stations are available in ACA, extrapolated values from GIS databases were preferred to infer the climate parameter controlling the brGDGT distribution. Using GIS `R` packages (`rgdal`, version 1.6-7 and `raster`, version 3.6-30; Bivand et al., 2015; Hijmans et al., 2015), climate parameters were extracted from `worldclim2.1` (Fick and Hijmans, 2017) and the extrapolated Aridity Index (AI) from the `CGIAR` database, (version 2; Trabucco and Zomer, 2018) for each surface sample from the ACA. The parameters used include Mean Annual Air Temperature (MAAT), Mean Annual Precipitation (MAP), and seasonal variables such as the mean air temperature of Months Above Freezing (MAF), as well as Mean Precipitation and Temperature for the Cold and Warm Quarters (MPCOQ, MPWAQ, MTCOQ, and MTWAQ). The AI is

Table 2. Main GDGT indices discussed in this study with their formula, their main interpretations and their references.

Index	Formula	Proxy interpretation	References
MBT'_{5Me}	$= \dfrac{\mathrm{Ia} + \mathrm{Ib} + \mathrm{Ic}}{\mathrm{Ia} + \mathrm{Ib} + \mathrm{Ic} + \mathrm{IIa} + \mathrm{IIb} + \mathrm{IIc} + \mathrm{IIIa}}$	Temperature, soil moisture	De Jonge et al. (2014); Lin et al. (2024)
MBT'_{6Me}	$= \dfrac{\mathrm{Ia} + \mathrm{Ib} + \mathrm{Ic}}{\mathrm{Ia} + \mathrm{Ib} + \mathrm{Ic} + \mathrm{IIa}' + \mathrm{IIb}' + \mathrm{IIc}' + \mathrm{IIIa}'}$	Temperature, independent from pH, better in drylands	De Jonge et al. (2014); Yang et al. (2015); Dang et al. (2016b)
CBT_{5Me}	$= -\log\left(\dfrac{\mathrm{Ib} + \mathrm{IIb}}{\mathrm{Ia} + \mathrm{IIa}}\right)$	pH, precipitation	De Jonge et al. (2014); Duan et al. (2022)
CBT'	$= -\log\left(\dfrac{\mathrm{Ic} + \mathrm{IIa}' + \mathrm{IIb}' + \mathrm{IIc}' + \mathrm{IIIa}' + \mathrm{IIIb}' + \mathrm{IIIc}'}{\mathrm{Ia} + \mathrm{IIa} + \mathrm{IIIa}}\right)$	pH	De Jonge et al. (2014); Raberg et al. (2022b)
IR_{6Me}	$= \dfrac{\sum \mathrm{X}_{6Me}}{\sum \mathrm{X}_{5Me} + \sum \mathrm{X}_{6Me}}$	Salinity, pH	Raberg et al. (2022b)
IR_{7Me}	$= \dfrac{\mathrm{IIIa}'' + \mathrm{IIa}''}{\mathrm{IIIa} + \mathrm{IIIa}' + \mathrm{IIIa}'' + \mathrm{IIa} + \mathrm{IIa}' + \mathrm{IIa}''}$	Salinity	Wang et al. (2021)
IR_{6+7Me}	$= \dfrac{\mathrm{IR}_{6Me} + \mathrm{IR}_{7Me}}{2}$	Salinity	Wang et al. (2021)
IR'_{6+7Me}	$= \dfrac{0.5 \times (\mathrm{IIa}' + \mathrm{IIb}' + \mathrm{IIc}' + \mathrm{IIIa}' + \mathrm{IIIb}' + \mathrm{IIIc}') + \mathrm{IIIa}''' + \mathrm{IIa}'''}{\mathrm{IIa} + \mathrm{IIb} + \mathrm{IIc} + \mathrm{IIIa} + \mathrm{IIIb} + \mathrm{IIIc} + \mathrm{IIa}' + \mathrm{IIb}' + \mathrm{IIc}' + \mathrm{IIIa}' + \mathrm{IIIb}' + \mathrm{IIIc}' + \mathrm{IIIa}''' + \mathrm{IIa}'''}$	Salinity	Wang et al. (2021)

calculated using the formula Eq. (3):

$$\mathrm{AI} = 10000 \times \frac{\mathrm{MAP}}{\mathrm{MA[ET_0]}} \tag{3}$$

where $\mathrm{MA[ET_0]}$ represents the Mean Annual Reference Evapotranspiration (Trabucco and Zomer, 2018). It is noticeable that AI increases in humid environments and decreases in arid to hyper-arid systems. The ~~thresholds~~ cut-offs and colour scale for aridity classes (hyper-arid, arid, semi-arid, dry sub-humid, and humid) used in this study are detailed in Table S.3 and follow the classification defined by Nash (1999).

2.3 GDGT analytical methods

BrGDGTs were analysed (Fig. 2, step 2) following the laboratory protocol fully detailed in Dugerdil et al. (2021a) and Davtian et al. (2018). First, we ground approximately one cm^3 of the soil or lacustrine samples in order to weigh them after a 24-hour lyophilization process. Then, total lipid content (TLC) was extracted twice from the sample by microwave-assisted extraction (MAE) at a temperature of 70 °C using DCM:MeOH (3:1, v/v). Following Huguet et al. (2006), a known concentration of an internal standard (C_{46} GTGT) was added to each TLC to estimate the absolute concentration of each GDGT compound. The TLC was separated into two fractions by elution on SiO_2 a column with hexane:DCM (1:1, v/v) and DCM:MeOH (1:1, v/v). The polar fraction containing br- and isoGDGTs was then dried under N_2 before being re-dissolved in hexane:iso-propanol

(98:2) solvent prior to injection. Analyses were performed using a high-performance liquid chromatography coupled to mass spectrometry equipped with atmospheric pressure chemical ionization (HPLC/APCI-MS, Agilent 1260 Infinity coupled to a 6120 quadrupole mass spectrometer). The entire analytical process was carried out in the geochemistry laboratory LGLTPE at *ENS de Lyon*. GDGTs were detected using Single Ion Monitoring (SIM). The protonated molecules were detected at *m/z* 1302, 1300, 1298, 1296, 1292, 1050, 1048, 1046, 1036, 1034, 1032, 1022, 1020, 1018, and 744 (C_{46}). Finally, we manually integrated each br- and isoGDGT based on the *m/z* ratio and retention time in order to identify each compound of brGDGTs with their 5-, 6- (De Jonge et al., 2014), and 7-methyls isomers (Ding et al., 2016). Following De Jonge et al. (2014), the Roman numerals represent different GDGT structures. The 6-methyl brGDGTs are marked with an apostrophe after the Roman numerals to differentiate them from their 5-methyl isomers, and two apostrophes represent the 7-methyls (Ding et al., 2016). The measurement accuracy of the GDGT analysis method was assessed through the inter-calibration exercises conducted in 2023 (De Jonge et al., 2024b).

2.4   brGDGT indices calculation

Based on raw GDGT integrations, we calculated absolute concentrations expressed in $ng.g_{sed.}^{-1}$ (Huguet et al., 2006) and fractional abundances (FA; De Jonge et al., 2014) using a R routine (Fig. 2, step 3). The classical indices of methylation for 5- and 6-methyls (MBT'_{5Me} and MBT'_{6Me}) and cyclisation (CBT' and ~~CBT'_{5Me}~~ CBT_{5Me}), as well as, the isomer ratios (IR_{6Me}, IR_{7Me}, IR_{6+7Me} and IR'_{6+7Me}; Wang et al., 2021) are also calculated and summarized in Table 2. To avoid overloading this study with multiple indices, we do not assess the Degree of Cyclisation index (DC; Sinninghe Damsté et al., 2009), nor its updated version incorporating 5- and 6-methyl isomers (Baxter et al., 2019). Although the DC index more accurately reflects changes in the number of internal cyclopentane rings than the CBT index (which track both isomers and cyclisations), we focus solely on CBT, as it is more commonly used in brGDGT studies from drylands (Guo et al., 2021; Chen et al., 2021; Duan et al., 2022).

2.5   Database compilations

Two databases are compared in this study (Figs. 1 and 2, steps 4 and 5). The Arid Central Asian Data Base (ACADB, n = 761) gathers ~~new samples~~ samples from Dugerdil et al. (2025b) used to train machine learning calibrations, as well as samples collected from previously published studies, listed in Table 1 and Table S.2. Among them, the majority of the sites were already cleaned and homogenized by Raberg et al. (2022b). We appended the northern Iranian samples (Duan et al., 2020, 2022) and the Sibero-Mongolian samples that have already been published in Dugerdil et al. (2021a) as the New Mongolian–Siberian Database. This dataset gathers 43 different sites from the Baikal basin to the northern part of the Gobi Desert (Fig. 1B and geographical details on Fig. 1 from Dugerdil et al., 2021a). From Cromartie et al. (2025), we appended 22 samples from Armenia, which follow an altitudinal gradient from the Ararat plain to the high plateau surrounding Lake Sevan (Fig. 1B). The salinity and 7-methyl FAs from Chinese data were also added (Wang and Liu, 2021; Kou et al., 2022). Among the ACADB (n = 761), there are 560 soil and 201 lacustrine samples. In order to compare the ACADB results, we also compiled a global Worldwide brGDGT surface Data Base (WDB, n = 2709) based on Raberg et al. (2022b) and Kou et al. (2022).

2.6 Statistical treatment

2.6.1 Univariate and multivariate analysis

Using R (version 4.4.2; R Core Team, 2020), we performed univariate linear relationships and multivariate analyses to under-
stand environmental controls on brGDGT distributions (Fig. 2, step 7). The reliability of univariate relationships was inferred
by Pearson's r, coefficient of determination (R^2), adjusted-R^2 (R^2_{adj}), p-values, and Root Mean Square Error (RMSE). The
multivariate analyses were conducted with the `vegan` package on scaled data (version 2.6-8; Dixon, 2003) and included
Principal Component Analysis (PCA) on the brGDGT matrix and Redundancy Analysis (RDA) combining the brGDGT and
surface climate parameters matrixes (Dixon, 2003). PCA is an unconstrained ordination that reduces data dimensionality by
identifying axes (principal components) capturing the most variance. RDA is a constrained ordination that explains variation in
GDGTs using environmental variables. To meet the assumptions of linearity and normality required for both analyses, environ-
mental variables were standardized using the `scale()` function, while the FAs of each brGDGT compound were transformed
using the Hellinger transformation (Eq. 4), which down-weights dominant compounds.

$$
\text{FA} - \text{transformed}_{i,j} = \sqrt{\frac{\text{FA}_{i,j}}{\sum\limits_{j} \text{FA}_{i,j}}}
\tag{4}
$$

with $\text{FA}_{i,j}$, the FA of compound j in the sample i. Since the 7-methyl FAs are not available for all samples in the compiled stud-
ies, they were removed from the databases for multivariate analysis. To select the most reliable environmental driving factors
to apply into the RDA, a Variance ~~Factors analysis (VIFs~~ Inflation Factor analysis (VIF, a method highlighting the covariance
between factors) was performed on climate parameters and soil characteristics (pH and TDS) using the `vif.cca()` function
from the same R package. To limit the covariance between them, only environmental factors below a threshold (e.g., below 10;
Cao et al., 2014) were kept for the RDA analysis and the following steps of the statistical workflow. The configurations of the
two PCAs (for soil and lacustrine samples) were compared using a Procrustes rotation analysis (i.e., comparing the similarity
between PCA and RDA ordination patterns by rotating one configuration to best match the other) and a PROTEST significance
test (i.e., quantification of the fitting degree via permutation test) between the two PCAs using the package `vegan` (Dixon,
2003). The same method was applied to compare the RDA brGDGT vs. climate parameters for soil and lacustrine samples.
Finally, linear relationships inferred between brGDGT indices and environmental factors follow Pearson's correlation (only
coefficients of determination with p-value < 0.001 are displayed on figures).

2.6.2 Grouping factor analysis

Samples were grouped by pH, aridity, salinity, and sample type to evaluate the most influential ~~confounding~~ controlling factors.
The applied ~~thresholds~~ cut-offs to bin classes are displayed in Table S.3. To identify data grouping patterns in relation to
bioclimatic parameters, sensitivity analyses were conducted in R by calculating the determination coefficients (multiple R^2
and R^2 for groups above and below ~~threshold~~ cut-off values) across a continuous range of ~~thresholds~~ cut-offs. For example, pH
~~thresholds~~ cut-offs were tested from 4 to 11 in 0.01 increments. Multivariate Analysis of Variance (MANOVA) was performed

with the `manova()` function to detect the most important environmental factors driving the variance among the 15 brGDGT FA (only the 5- and 6-methyls were selected) and among the main GDGT indices (Fig. 2, step 8). Then, the univariate ANOVA results were obtained with `summary.aov()` for each brGDGT compound and index. Both functions come from the `stats` R base package (version 4.4.2; R Core Team, 2020). The MANOVA tests for differences in multiple dependent variables across different groups to see if group means are significantly different, while the ANOVA tests for differences in the means of a few groups to determine if at least one group mean is significantly different. The assumption of multivariate normality was tested with Mardia's Skewness and Kurtosis tests (i.e., MANOVA is possible only if the two *p*-values are higher than 0.05; Mardia, 1970). The assumption of homogeneity of variance-covariance was tested for each variable and each grouping factor using the Levene's test (Bierens, 1983). Using the most relevant ~~confounding~~ controlling factors, specific $\text{MBT}'_{5\text{Me}}$-based temperature calibrations were done for each grouping factor. To compare the linear relationship among groups, the significance of the difference was carried out with the *z*-statistic following Clogg et al. (1995), Eq. (5):

$$z = \frac{\beta_1 - \beta_2}{\sqrt{\text{SE}_1^2 + \text{SE}_2^2}} \tag{5}$$

with β_n the coefficients and SE_n the standard errors of the linear regressions among the *n* groups. The *p*-values for the *z*-statistics are inferred with a normal distribution. The same *z*-statistic approach [Eq. (5)] was applied to determine the significance of the difference between each linear model intercept (i.e., here, the offset between each calibration). The *z*-statistic was preferred to the ~~t-test since the size of the data is high~~ *t*-test since the number of samples is large (e.g., more than 30 samples; Moore et al., 2009). All statistical treatments and graphical representations (except the map done with `QGIS 3.34 Pritzen` and the methodological workflow done with `Inkscape`) were performed in R. The plots were designed with the `ggplot2` package (version 3.5.1; Wickham, 2016) and, more particularly, the `ggtern` (version 3.5.0; Hamilton and Ferry, 2018) for the ternary diagram (Fig. 2, step 6).

3 Results

3.1 brGDGT distribution

3.1.1 brGDGT concentrations

The brGDGT absolute concentrations are estimated from the C_{46} internal standard method. To avoid biases from instrument drift (Huguet et al., 2006), only the samples analysed in the geochemistry laboratory LGLTPE at *ENS de Lyon* are described here. The dataset gathers 234 samples from Armenia, Azerbaijan, China, Mongolia, Tajikistan, Russia and Uzbekistan, published in Dugerdil et al. (2021a), Cromartie et al. (2025) and Dugerdil et al. (2025a). The brGDGT concentration is heterogenous among the ~~ACA surface samples~~ dataset, and it mainly depends on the sampling site location and sample type. ~~They vary~~ It varies between 674 ± 2825, 87 ± 314 and 342 ± 1822 $\text{ng.g}^{-1}_{\text{sed.}}$ for lacustrine, soil and the whole ~~database~~ dataset, respectively. Lacustrine samples are much richer in brGDGT than soil samples (about ten times more concentrated). Among the soil samples, the more moisture in the soils, the higher the concentrations, from 149 ± 594 to 24 ± 33 $\text{ng.g}^{-1}_{\text{sed.}}$. From

~~drylands~~hyper-arid and arid environments, samples from sand dunes are poorer than loess, silt-rich, and *solonchak* samples. They are close to the detection level (i.e., integration peaks smaller than twice the noise level), thus increasing uncertainties for indices based on 6- and 7-methyls.

3.1.2 brGDGT fractional abundances

The brGDGT distribution is described from soil (Fig. 3A) and lacustrine samples (Fig. 3B). FAs for lowest abundances (i.e., mean value below 5%) are given in panels A1–B2. With regard to FAs in soil samples, the prevalent compounds are IIa' (mean value $\simeq$ 30%), IIIa' ($\simeq$ 22%), Ia ($\simeq$ 14%), IIa ($\simeq$ 10%) and IIIa ($\simeq$ 6%, Fig. 3A). In lacustrine samples, the distribution is dominated by IIIa' ($\simeq$ 19%), IIa' ($\simeq$ 16%), Ia ($\simeq$ 12%), IIa ($\simeq$ 10%) and IIIa ($\simeq$ 9%, Fig. 3B). In contrast, compounds such as IIIb, IIIb', IIIb", IIIc, IIIc', IIb", IIc, and IIc' are rare in both soil and lacustrine samples, with average abundances ranging from 1% to 2% ~~.~~ (Fig. 3A1–B2). It is noteworthy that, for each compound, the 6-methyl isomers are more abundant than the 5-, and the 5- are more abundant than the 7-. ~~This trend~~ The higher median values for the 6- over the 5-methyl isomers is more marked for soil than lacustrine samples. The 7-methyl isomers ~~have higher importance~~ are more abundant in lacustrine than in soil samples. For both sample types, the ~~histograms~~ boxplots reveal that brGDGT distributions vary across the different aridity classes, with ~~trends emerging with increased aridity :~~ median FAs shifting toward higher values with drier aridity classes: median IIIa increases in the humid ~~group~~class, while IIIa' and IIIa" are higher in the arid and hyper-arid ~~groups~~classes. A similar ~~trend~~ median shift is observed between IIc and IIc'. Additionally, IIa increases with ~~humidity~~wetter aridity classes, while the IIa' distribution remains largely insensitive to changes in aridity classes for lacustrine but decrease with higher humidity for soil samples. Compounds Ia, Ib and Ic exhibit discernible variations between aridity classes, although the observed ~~trends~~ shifts are not unequivocal. Finally, aridity control is less evident in other low-abundance compounds, including the IIIb, IIIc, and IIb, and all 7-methyl isomers.

3.1.3 Methylation distribution

In soil samples from the ACADB, tetra-, penta-, and hexamethylated brGDGTs range from 0 to 55%, 20 to 80%, and 0 to 85%, respectively (Fig. 4A1 and A2). The distribution of hexamethylated compounds is the most variable in ACA. By contrast, in the WDB, brGDGT distributions are strongly centred around tetramethylated compounds, with only a few samples showing high hexamethylated fractions; the majority contain less than 20% of hexamethylated compounds. About the aridity effect, ACADB samples from a humid environment fit the WBD distribution better, while arid and hyper-arid samples shift towards lower tetramethylated content.

Similarly, for lacustrine samples (Fig. 4B1 and B2), the ACADB shows tetramethylated brGDGTs ranging from 0 to 60%, pentamethylated from 10 to 85%, and hexamethylated from 10 to 90%. Compared to WDB, the *croissant shape* of the ternary distribution is retained but shifts towards less tetra- and more pentamethylated forms. For lacustrine samples, the ~~aridity effect seems mitigated compared to~~ distribution across aridity classes appears less contrasted than for soil samples. However, the samples from humid environments are spread along a bimodal distribution following the hexamethylated axis, while this is not the case for hyper-arid to dry sub-humid samples with hexamethylated above 20%.

3.1.4 brGDGT multivariate spaces

PCAs were performed on 400 soil and 361 lacustrine surface samples, using Hellinger-transformed FA values (Fig. 5A and B). The brGDGT loadings for the first and second components explain 42% and 18% for soil samples and 40% and 19% for lacustrine samples, respectively. For both, the most important contributing compounds are IIIa', IIa, IIa', and Ia, followed by IIb', IIIa, IIIb', IIc', and IIIc'. PCA_1 corresponds to a gradient between the 5- and 6-methyl isomers, with positive loadings for IIa, Ia, Ib, and IIIa and negative loadings for IIa', IIIa', and IIb'. PCA_2 follows a gradient marked by the number of internal cyclisation: the positive loading is driven by compounds with one or two internal cyclisations (mainly IIb', IIIb', IIIc', and IIc'), while the negative loading presents compounds without internal cyclisation (Ia and IIa'). About the distribution of aridity classes over this multivariate space (highlighted by the upper and lateral sample densities in Fig. 5~~), a clear~~ A and B), the data distribution suggest that an aridity gradient can be superimposed on the isomer gradient (i.e., along PCA_1 with humid samples on a positive loading and hyper-arid samples on a negative one). This gradient is clearer for soil than for lacustrine samples. In between, arid, semi-arid, and dry sub-humid samples show a higher internal cyclisation number (positive PCA_2), giving a *triangular* shape to the sample distribution.

Procrustes rotation analysis, along with the PROTEST *r* and *p*-values, was used to assess the similarity between the two PCAs (Fig. 5C). The statistical results reveal that the brGDGT multivariate space is very similar for soil and lacustrine samples with $m_{12}^2 = 1.05$, $r = 0.91$ and *p*-value < 0.01. The more variable components between soil and lacustrine multivariate spaces are IIIa', IIa, and Ib. It is noteworthy that Ib is correlated with IIb and IIIa in soils, while it is correlated to Ia in lacustrine samples.

3.2 brGDGT responses to environmental controls

3.2.1 ACA bioclimate multivariate space

~~When~~ The selection of bioclimatic parameters that can be reliably reconstructed from fossil proxies is essential (Salonen et al., 2019). To evaluate this, we conducted (1) a multivariate analysis on `worldclim2.1` data extracted at the ACADB sampling locations, to identify the primary and secondary bioclimatic gradients and their main parameter contributors, and (2) a Variance Inflation Factor (VIF) analysis to quantify multicollinearity within the brGDGT–bioclimate multi-variate space of the ACADB. The goal is to confirm which bioclimatic parameters are the most informative and ensure they are as statistically independent as possible, in order to minimize biased climate reconstructions.

First, when considering the bioclimate space of ACA sampled at the ACADB sampling points (Fig. 1E), the main loading (PCA_1 = 53%) is a temperature gradient and the secondary loading (PCA_2 = 29%) is a precipitation gradient. About the climate parameter contribution, AI and MAP have more influence on the ACA bioclimate variance, followed by MPCOQ and MAAT. In ACA, all temperature parameters are strongly correlated, indicating that temperature seasonality is roughly homogeneous within the ACADB. This observation is consistent with the lower variance explained by MAF than MAAT. The coefficient of variation among the ACADB is higher for MAAT than seasonal temperature parameters (170 vs. 30%). Contrarily, Mean Precipitation of Warm / Cold Quarters (MPWAQ and MPCOQ, respectively) are negatively correlated, showing a

split in seasonal precipitation patterns among the ACADB, which is in line with the global climate observations in ACA (Chen et al., 2024).

~~In order~~ Then, to verify that these parameters remain the primary factors to explain the brGDGT variance space, ~~Variance Factor (VIF)~~ VIF analyses were performed on two models: (1) using all environmental parameters (i.e., all climate parameters, altitude, pH, and salinity) and (2) only a selection of climate parameters to verify that VIFs < 10 (Cao et al., 2014). In Table S.4, the multicollinearity between MAAT, MTCOQ, and MTWAQ is clear (VIFs > 159.1) and reduced with MAF (VIF = 26.7). Multicollinearity is lower among the precipitation parameters (VIF < 37.8). When keeping only AI, MAAT, MAF, MPCOQ, pH, and salinity, all VIFs are below 6. VIFs for pH and salinity do not change between the two models, showing their independence from climate parameters. Finally, from the total set of environmental variables, the VIF analysis removed the altitude, MAP, MPCOQ, MTCOQ, and MTWAQ. The remaining environmental parameters have $VIF_{MAAT} = 6$, $VIF_{MAF} = 4.5$, $VIF_{MPCOQ} = 2.1$, $VIF_{AI} = 1.5$, $VIF_{pH} = 1.5$ and $VIF_{Salinity} = 1.3$.

3.2.2 Controls on brGDGTs in the ACA bioclimate space

Regarding the environmental controls on brGDGT distribution, RDAs were performed based on analyses of 113 soil and 67 lacustrine samples (excluding samples without pH and salinity data), including 15 brGDGT compounds (limited to 5- and 6-methyl isomers) and six environmental variables (Fig. 5D and E). The first two RDA axes explained 20% and 5.9% of the variance in soil samples, and 22% and 3.4% in lacustrine samples. The overall correlation between the brGDGT composition and the environmental variables was 0.31 for soils and 0.27 for lakes. About the distribution of sites and brGDGT vectors, we observe the conservation of the distribution between PCA and RDA for soil (Fig. 5A and D): similar PCA_1 and RDA_1 loadings, and reverse loading among RDA_2 and PCA_2.

The distribution of soil samples in the RDA ordination reflects a gradient of aridity (Fig. 1D), with humid samples on positive loading associated with high AI and salinity and hyper-arid samples on negative one correlated with pH, MAF, and MAAT. This gradient corresponds to a predominance of GDGT compounds IIIa', IIIb', and IIa' in arid samples, while more humid sites are associated with higher FAs of IIa and Ia. Thus, the aridity gradient along the RDA_1 loading is clearly conserved from PCA to RDA. Surprisingly, higher salinity is associated with higher AI (i.e., humid conditions) and negatively correlated with pH (i.e., acidic conditions). Although soil salinity is expected to increase under bioclimatic aridity (Muhammad et al., 2008), our results show that in ACA, salinity is largely independent of climate parameters (Fig. 1~~E~~D).

For lacustrine samples (Fig. 1B and E), the loadings are quite different between PCA and RDA, mainly due to low IIa and IIa' correlations with environmental parameters in RDA (despite their strong importance in primary and secondary loadings in PCA). The aridity gradient is not clear (mainly due to the scarcity of hyper-arid and humid lacustrine samples). Here, salinity is negatively correlated with pH and AI. Additionally, tetramethylated compounds (Ia, Ib, and Ic) are controlled by both temperature (MAAT and MAF) and salinity.

The Procrustes rotation analysis carried out on the two different RDAs (Fig. 5F) shows that the correspondence between the two RDA spaces is smaller than between the two PCA spaces (Fig. 5C) with $r = 0.67$ and p-value < 0.003. Compounds IIIa and IIa exhibit the most pronounced rotations (i.e., the differences in their loadings between the two PCAs as revealed by the

Procrustes rotation analysis), indicating substantial differences in environmental controls between soil and lacustrine samples.

395 For environmental parameters, salinity and AI are the two parameters with the highest degree of rotation between the soil and lacustrine RDA spaces. AI is more contributing in the soil samples RDA, while salinity is more contributing in the lacustrine samples RDA.

3.2.3 Methylation indices relationships to climate parameters

Linear relationships between the two main indices of methylation generally used in brGDGT calibration studies, the MBT'_{5Me}

400 and MBT'_{6Me}, are tested against pH, AI, MAAT, and salinity (Fig. 6). The R^2 (*** indicates p-value < 0.001) are given for each relationship and for both subsets of sample type (i.e., soil and lacustrine samples). For soil samples, the strongest MBT'_{5Me}-based linear relationship is related to MAAT ($R^2 = 0.31$***), even if it is also associated with pH ($R^2 = 0.17$***) and AI ($R^2 = 0.15$***). The relationship with salinity is, however, not significant. Contrarily, for lacustrine samples, salinity exhibits the strongest relationships with MBT'_{5Me} ($R^2 = 0.31$***). Correlation coefficients obtained with MBT'_{6Me} are generally lower

405 than those with MBT'_{5Me} with pH for soils ($R^2 = 0.11$***) and with MAAT for lacustrine samples ($R^2 = 0.13$***). When statistically significant, all relationships follow similar trends (positive or negative) for MBT'_{5Me} and MBT'_{6Me}.

Comparing the ACADB to the WDB in Fig. 6, some relationships are similar: MBT'_{5Me} with MAAT and salinity, and MBT'_{6Me} with pH and AI, despite the tighter climatic range of ACADB compared to WDB. Contrarily, some trends are reversed: MBT'_{6Me} with salinity and MBT'_{5Me} with pH. It is also noticeable that ACADB samples from humid and dry sub-

410 humid conditions fit better with the WBD distribution than arid and semi-arid systems. ~~Hyper-arid samples often have extreme values.~~

3.2.4 Cyclisation, isomerisation, and pH

The cyclisation and isomer indices (here, CBT', ~~CBT'$_{5Me}$~~ CBT$_{5Me}$, IR$_{6Me}$ and IR'$_{6+7Me}$), which are commonly considered to be pH-related proxies, are tested against aridity, pH and salinity on WBD and ACADB. On the ACADB, the linear relationships

415 between pH and these indices are not significant for lacustrine samples (Fig. 7). In soil samples, isomer ratios appear to correlate more strongly with pH than cyclisation indices, with IR$_{6Me}$ showing the highest explanatory power ($R^2 = 0.27$***). This pattern is consistent in both the WDB and ACADB datasets. About the cyclisation, CBT' is more linearly related to pH than ~~CBT'$_{5Me}$~~ CBT$_{5Me}$. However, both indices suffer from a relation break around a pH threshold of 7.3 (highlighted by dashed lines on Fig. 7A and B). This indicates that the cyclisation degree is linearly correlated to pH only in acidic samples. To test the

420 pH threshold value, the CBT' vs. pH linear relationship was tested for the two groups, below and above the threshold, using a continuous implementation of ~~threshold~~ cut-off pH from 4 to 11, with 0.01 steps each (Fig. S.2). The best R^2 is for a pH of 7.3, with multiple R^2 of 0.45 for overall soils, 0.54 for acidic soils, and 0.05 for alkaline soils. Similar ~~thresholds~~ cut-offs are also observable with aridity and salinity, although with lower regression strength (R^2 of 0.15*** and 0.09***, respectively). Finally, ~~there is a strong similarity between~~ the CBT'-IR$_{6Me}$ and CBT'-IR'$_{6+7Me}$ relationships are more similar in term of

425 slope and correlation for soil than lacustrine samples (R^2 of 0.87*** and 0.80*** ~~) for soils, while this does not hold true for lacustrinesamples (~~for soil, 0.80*** and 0.13*** for lacustrine, respectively in Fig. 7G and H).

3.2.5 Isomer ratios responses to aridity and salinity

The common isomer ratios used to infer salinity are tested with aridity and salinity (Fig. 8). The linear relationships between IRs and MBT'_{6Me} are also tested. For salinity, the correlations are more statistically significant with lacustrine than with soil samples, by order of strength: IR'_{6+7Me} ($R^2 = 0.41$***), IR_{7Me} (0.40***) and IR_{6+7Me} (0.37***). For soil, IR_{6Me} has the strongest relationship with pH ($R^2 = 0.09$***), but the relationships with aridity are also significant, especially with IR_{6+7Me} ($R^2 = 0.17$***). The relationships are comparable between ACADB and WDB, although the WDB environmental range is wider, especially for low salinity and high AI values. IR'_{6+7Me} is slightly correlated with the MBT'_{5Me} index in lacustrine samples ($R^2 = 0.29$***), while it is more significantly correlated to MBT'_{6Me} in soil samples (0.58***). These relationships are similar in WDB, although no linear relationship appears between IR'_{6+7Me} and MBT'_{5Me} in WDB. Moreover, the isomer ratio relationship with salinity drastically changes depending on the relative weight given to 7-methyl isomers. The regression between IRs and salinity shows increasing explanatory power with 7-methyls weight, with R^2 values rising from 0.08 for IR_{6Me} to 0.40 for IR_{7Me}, and from 0.37 for IR_{6+7Me} to 0.41 for IR'_{6+7Me}. This is mainly due to the salinity's positive correlation with 7-methyls and negative one with 6-methyls (respectively, Pearson's r of 0.64 and -0.35, Fig. S.3).

3.3 Robustness of the analysis of variance between groups

Since it was previously shown that the different environmental parameters have different interactions in the brGDGT distribution worldwide and in the ACA (Yang et al., 2014; Deng et al., 2016), both on soil and lacustrine samples, we evaluate the strength of each driving factor. Since the *sample type* group is a qualitative factor, the other quantitative factors (i.e., bioclimate and physicochemical parameters) were also binned into qualitative groups (see Table S.3 for the ~~thresholds~~ cut-offs used for binning). The two MANOVA models inferred to evaluate their differential influences on (1) FAs distribution and (2) indices from the ACADB are displayed in Table 3.

3.3.1 Analyses of variance for the FAs

This first MANOVA tests the response of the 15 brGDGT FAs to the four grouping factors: aridity, pH, salinity, and sample type. MANOVA results (in terms of F-statistics and p-values) are given in the first row of Table 3 while ANOVAs for each compound is given in rows two to 16. Levene's test p-values are provided in Table S.5. The higher MANOVA F-statistic (with a p-value < 0.001, symbolized by the *** symbol) represents the stronger environmental parameter to separate FA into groups. First, it appears that the sample type ($F = 10.2$***) is the most influential grouping factor on the FA variance, followed by salinity (7***) and pH (6.5***). Moreover, the sample type is responsible for the clustering among IIIa, IIIb, IIb, and Ic, while pH mainly influences IIa', IIa, Ic, and IIIa', and salinity influences IIIa, IIIa', IIIc, and IIb'. Aridity plays a role mainly on IIa, Ia, and IIIa'. Generally, the main compounds are impacted in their distribution by all ~~confounding~~ controlling factors.

Table 3. Statistical results (approximate *F*-statistics and *p*-values) of the two MANOVAs carried out to test the brGDGT (1) FAs and (2) indices responses to environmental classes (i.e., aridity, pH, salinity, and sample type). The MANOVA *F*-statistics are presented in the first row of the two models, followed by the *F*-statistics of the univariate ANOVA for each item (i.e., each FA and each index). The significance is given by the number of stars[a]. The samples without pH or salinity measurements were removed from the analysis (i.e., n = 328). The *p*-values from Levene's test, which are important for assessing the reliability of the MANOVAs, are provided in Table S.5.

Model	Compound	Aridity	pH	Salinity	Sample type
Model 1	**F-statistics**	3.4***	6.5***	7***	**10.2***[b]**
(FAs)	f(IIIa)	1.7	3.6*	**29***	**38.2***
	f(IIIa')	10.8***	9.6***	14.7***	6.5*
	f(IIIb)	0.7	2.4	1.4	25.8***
	f(IIIb')	2.3	2.8	1.2	1.4
	f(IIIc)	1.2	6.1**	9.8***	1.7
	f(IIIc')	0.9	1.9	2.7*	0.4
	f(IIa)	**22***	15.7***	2.9*	1.5
	f(IIa')	2.2	**18.5***	13.9***	4.6*
	f(IIb)	0.6	4.4*	2.5	20.2***
	f(IIb')	1.3	11.5***	6.6***	10.3**
	f(IIc)	1.7	1.8	0.8	0.5
	f(IIc')	1	5**	1.5	1
	f(Ia)	18.5***	6.7**	4.7**	4.1*
	f(Ib)	1.4	2.2	2.5	0.9
	f(Ic)	3.7**	12.7***	0.8	13.9***
Model 2	**F-statistics**	5.7***	8.4***	**9.1***	8.4***
(Indices)	MBT'_{5Me}	6***	7.2***	17.7***	**37.1***
	MBT'_{6Me}	11.9***	8***	13***	1.3
	IR_{6Me}	13***	11.3***	9.9***	5.4*
	IR_{6+7Me}	24.8***	6.1**	13.9***	1
	IR'_{6+7Me}	**28.1***	3.5*	**18.9***	0.5
	CBT'	13.7***	**13.4***	8.7***	2.3
	~~CBT'_{5Me}~~ CBT_{5Me}	5***	4.8**	0.6	4.4*

[a] The *p*-values are expressed in terms of *stars* with *** for $p \leq 0.001$, ** $p < 0.01$, * $p < 0.05$ and nothing for not-significant *F*-statistic (i.e., *p*-value ≥ 0.05). [b] The highest *F*-statistic for each MANOVA and ANOVA is displayed in bold text.

3.3.2 Analyses of variance for the brGDGT-based indices

Since the majority of brGDGT applications are based on traditional indices, the response of MBT'_{5Me}, MBT'_{6Me}, IR_{6Me}, IR_{6+7Me} and IR'_{6+7Me} to aridity, pH, salinity, and sample type was tested in the second MANOVA (line 16 of Table 3 followed by the ANOVA statistical results for each index). For MANOVA, the most important grouping factor is salinity (*F* = 9.1***), followed by pH and sample type (8.4***). Aridity is the weakest grouping factor (5.7***). The graphical representation of the variance for each group is available in Fig. S.4. More specifically, for MBT'_{5Me}, the variance is mainly explained by sample type (37.1***) and salinity (17.7***). For MBT'_{6Me}, the variance is mainly explained by salinity (13***) and aridity (11.9***). IR indices show stronger clustering based on aridity and salinity than on pH or sample type. Aridity and salinity gradients are clear among groups for IR_{6+7Me} and IR'_{6+7Me} while IR_{6Me} variance is more steady. For all three indices, there is

460

a clear distinction for hypersaline and humid group variance (low index value for humid groups and high value for hypersaline). ~~CBT'$_{5Me}$~~ CBT$_{5Me}$ have a similar variance for each group, while CBT' is clustered by aridity and pH (13.7*** and 13.4***).

4 Discussion

Comparing the ACADB results with other studies, the question of the relative importance of the confounding factor on ~~past~~ brGDGT palaeothermometer applications from drylands is raised. The effects of the confounding factors on the past temperature estimation, such as pH (mainly for extrema; Duan et al., 2020), aridity, seasonality, and salinity, are currently studied in ACA (Guo et al., 2021; Chen et al., 2021; Kou et al., 2022; Duan et al., 2022). More generally, the impact of ~~confounding~~ controlling factors on geochemical proxies used to reconstruct palaeoenvironmental changes has been increasingly recognized in brGDGT-based temperature calibrations (De Jonge et al., 2014; Häggi et al., 2023). Mainly, based on the ACADB results, we discuss (1) the impact of these factors on brGDGT indices (methylation, isomer and cyclisation indices); then (2), the complex interaction between ~~confounding~~ controlling factors; (3) the applicability of former and new calibration depending on confounding factor classes; and (4), we provide recommendations for their applicability in the past brGDGT archives in drylands. We will first focus on the reliability of MBT'$_{5Me}$ and MBT'$_{6Me}$ to reconstruct past MAAT and on isomer or cyclisation indices to infer salinity and pH in drylands. The following discussion is mainly based on ACADB results from linear regressions, as well as multivariate and variance analyses. However, due to limited metadata availability, these integrative statistical approaches (RDAs and MANOVAs) were applied to a reduced dataset (113 soil and 67 lake samples), and further research is needed to confirm the conclusions drawn.

4.1 Applicability of brGDGT-based proxies

4.1.1 ~~*MBT'$_{5Me}$*~~ MBT'$_{5Me}$ responses to temperature

The analysis of the ACADB climate space, based on the PCA (Figure 1E) and RDAs (Figure 5D and E), indicates that MAAT better captures both the climate variability and the brGDGT response across ACA compared to MAF. In both datasets, the proportion of variance explained by MAAT exceeds that explained by MAF, with the only exception being brGDGT assemblages from lacustrine samples. Based on this, we focus the discussion on MAAT, even though MAF is often preferred in brGDGT studies due to its relevance for representing the bacterial growing season (Deng et al., 2016; Dearing Crampton-Flood et al., 2020). However, the actual timing of bacterial growth may depend not only on temperature, but also on soil water availability (Lei et al., 2016). This is particularly relevant in the ACADB region, where MAF generally aligns with summer across ACA, while soil moisture availability is not spatially synchronous, with rainfall peaks in spring and autumn in eastern ACA, and in summer in the western part (Figure S.1).

When considering the MBT'$_{5Me}$-MAAT relationships in the ACADB, the determination coefficients for both soil and lacustrine samples are limited (Fig. 6). The linear correlation is significantly higher in semi-arid to humid soils than hyper-arid and arid soils (Figs. S.8), in line with Wang et al. (2019). This ~~attenuation~~ weakening of the MBT'$_{5Me}$-MAAT correlation is

also well observed on lacustrine samples where MBT'_{5Me} is more correlated to salinity than to MAAT (Fig. 6E and G) in line with Liang et al. (2024). In drylands, MBT'_{5Me} is also correlated with soil water content (Dang et al., 2016b). However, numerous temperature reconstructions use the MBT'_{5Me} index to capture the brGDGT compound's response to temperature (De Jonge et al., 2014; Chen et al., 2021), even if several studies have shown a strong bias in MBT'_{5Me}-temperature relationship under arid conditions (Sun et al., 2019; Dugerdil et al., 2021a). Guo et al. (2021) demonstrated that in arid environments, the relationship between temperature and brGDGT methylation differs between 5- and 6-methyl isomers. The dominance of Actinobacteria and Verrucomicrobia, each linked to distinct 5- and 6-methyl brGDGT signatures, in arid soils may help explain the limited effectiveness of the MBT'_{5Me} index in capturing climate signals within the ACADB. In this context, MBT'_{5Me}-based temperature calibration in drylands may have reduced reliability. Among solutions to improve this type of calibration, specific MBT'_{5Me}-based temperature calibration can be provided for specific confounding factor classes.

4.1.2 MBT'_{6Me} responses to climate

MBT'_{6Me}-MAAT trends opposite for the WDB compared to the ACADB (Fig. 6F), even if the correlations with temperature remain weak. The correlation is slightly better with AI (Fig. 6D). The MBT'_{6Me} index has been proposed as a reliable temperature proxy when MAP and MAAT are negatively correlated (Guo et al., 2021), a condition not met in the ACADB dataset. From the ACADB, we can estimate that MBT'_{6Me} is slightly more controlled by AI than MAAT. Moreover, the tetramethylated compounds (which are the major compounds involved in MBT'_{5Me} and MBT'_{6Me}, De Jonge et al., 2014) are not as important in ACADB as in WDB (Fig. 4A). Additionally, the climate response of tetramethylated compounds is not clear in ACADB (Fig. 5D), while the IIa' is well correlated with MAAT. Initially designed by De Jonge et al. (2014) as a methylation index for tetramethylated over the sum of tetramethylated plus 6-methyl isomers, the MBT'_{6Me} is understudied. However, Wang et al. (2016) and Guo et al. (2021) observed in arid soils that the MBT'_{6Me} has a better response to temperature and aridity changes than the MBT'_{5Me}. Also, their studies show an opposite correlation with MAAT than in global soil datasets, in line with our results.

4.1.3 Complementarity of MBT'_{5Me} and MBT'_{6Me} to infer aridity

We propose to use the difference between MBT'_{5Me} and MBT'_{6Me} to track past aridity change, since it was shown that MBT'_{6Me} variance is similar to that of MBT'_{5Me} under humid conditions, while it is smaller under hyper-arid to dry sub-humid conditions (Fig. 9A and B). This observation holds true in both soil and lacustrine samples. Therefore, following the trends of these two indices in the past could allow distinguishing between periods of constant humid conditions, whenever they are correlated with similar variance, and that of constant or shifted arid conditions (not correlated). Moreover, the current MBT'_{5Me}-AI correlation is negative (Fig. S.5A), while the MBT'_{6Me}-AI correlation is positive (Fig. S.5B), and similar to the soil water content effect on MBT'_{6Me} (Dang et al., 2016b). Then, the $\Delta(MBT'_{5Me}, MBT'_{6Me})$ gives a quite reliable estimation of the AI (i.e., the difference between the two indices, Fig. S.5C). This approach is more appropriate for soil than lake samples, since the MBT'_{6Me} distribution in lacustrine samples is correlated with MAAT rather than AI (Fig. 6D and F), making the MBT'_{6Me}-based calibration more accurate than the MBT'_{5Me} one in ACA lakes.

The statistical independence between AI and MAAT has to be verified, especially since AI is related to temperature via the Mean Annual Reference Evapotranspiration (cf. Eq. (3) and Trabucco and Zomer, 2018). Among ACADB, MAAT and AI are independent bioclimatic variables (R^2 below 0.01 for lacustrine and about 0.15 for soil samples). Moreover, focusing only on soil samples, the $\Delta(\mathrm{MBT}'_{5Me}, \mathrm{MBT}'_{6Me})$-AI relationship has been tested for similar MAAT values (Fig. 9C). The regressions across MAAT classes are generally consistent, except at the extremes of the Aridity Index. The higher multiple R^2 compared to the global model indicates that the relationship between $\Delta(\mathrm{MBT}'5Me, \mathrm{MBT}'6Me)$ and AI is largely independent of MAAT. When comparing this result with previous studies, we found similar MBT'_{5Me} and MBT'_{6Me} behaviour compared to MAAT (correlations positive for MBT'_{5Me} and negative for MBT'_{6Me} in Guo et al., 2021). This is also supported by the evidence that MBT'_{6Me} is correlated with AI and soil water content (Dang et al., 2016b; Guo et al., 2021). Although the difference between ratios is still not commonly used for brGDGTs, this approach is increasingly applied to other geochemical proxies of past climate parameters (Hällberg et al., 2024).

4.1.4 Controls of salinity on isomer ratios

Salinity is a major ~~confounding~~ controlling factor in ACA, impacting both brGDGT distribution in the environmental space (Fig. 5B and E) and the variance of FA and indices (Table 3). It is also significant that the salinity could be monitored through isomer content (Fig. 8). Mainly, the IR'_{6+7Me} appears to be the more reliable index to track salinity gradients among lacustrine ACADB samples, in line with Wang et al. (2021) and Kou et al. (2022). These studies have revealed the unusual over-representativeness of 7-methyl compounds in brackish to hypersaline lacustrine lakes, like in the ACADB. Wang et al. (2021) also reported a slight impact of salinity on IR_{6Me} which may be due to pH-salinity covariation in their database. Since pH and salinity are not covarying in the ACADB soils, it explains why IR_{6Me} is less correlated with salinity for ACADB soils (Fig. 8A). However, the two factors are covarying in the lacustrine dataset. This could explain why IR_{6Me}-salinity regressions are similar between soils and lacustrine samples (R^2 about 0.08) while IR'_{6+7Me} is not. We conclude that (1) the unusual over-representativeness of 7-methyl due to salinity is important in lakes but not significant in soils, and (2), IR'_{6+7Me} is the more reliable brGDGT index to track salinity changes in both sample types.

~~Especially for lakes,~~ IR_{6Me} is well correlated with salinity for low salinity values, particularly in lacustrine samples (i.e., mainly fresh-water lakes, Fig. 8A and Wang et al., 2021), while IR_{7Me} is more significant for higher salinity ranges (Fig. 8B). ~~These thresholds of salinity classes are~~ Below TDS values of ca. 1,000 mg.L^{-1}, the IR_{6Me}–salinity relationship show lower data dispersion that above this threshold (Fig. S.6A). For the IR_{7Me} index, a saturation effect due to low 7-methyls isomer mitigate the IR_{7Me}–salinity relationship, below TDS values of ca. 11,000 mg.L^{-1} (Fig. S.6B). The different IR response to salinity below and above these salinity thresholds (TDS $\in$ [1,000; 11,000] mg.L^{-1} in Fig. 8A and B) is attenuated when both 6- and 7-methyls are included in the ratio over 5-methyls (i.e., IR_{6+7Me} and IR'_{6+7Me} indices, Fig. 8C and D). Mainly, lake salinity conditions may impact the *in situ* bacterial community responsible for the 6- and 7-methyl over-abundances (Liang et al., 2024). The ACADB validates the use of IR'_{6+7Me} as a salinity proxy proposed by Wang et al. (2021), in complement to previous proxies such as dinoflagellate cysts (Leroy et al., 2013), diatoms (Unkelbach et al., 2020), archaeol, and caldarchaeol ecometric (Kou et al., 2022) or extended archeol (So et al., 2023).

4.1.5 Controls of pH on isomer ratios and cyclisation degree

Historically, brGDGT-based pH reconstructions were mainly conducted through cyclisation indices (e.g., CBT' and CBT_{5Me}, De Jonge et al., 2014). However, more and more studies highlight that the isomer ratio is also well correlated with pH changes (Dang et al., 2016a; De Jonge et al., 2024a). From the ACADB, it appears that pH impacts the isomers more than the cyclisation content (i.e., IR_{6Me} seems to be a more reliable proxy for pH than CBT' in ACA, Figs. 7 and 8). This is consistent with the Inner Mongolian aridity transect study (Guo et al., 2021). At the global scale, CBT' presents a slightly higher correlation with pH than IR_{6Me}, but the sample type effect is stronger on CBT' (i.e., calibration for different sample types are more different in slope and intercept for CBT' than IR_{6Me}, Raberg et al., 2022a). IR_{6Me} may be more robust to infer past pH in a context of shifting sedimentary flux. Particularly, panels (A) and (B) from Fig. 7, show that the cyclisation indices ~~suffer from a correlation disruption for alkaline soils. Here, a threshold~~ exhibits a piecewise, dual-slope response across a threshold, indicating a non-linear, threshold-dependent relationship rather than a single unified pH control. The threshold appears after pH > 7.3 (threshold found by sensitivity analysis, Fig. S.2), in line with a pH > 7.5 threshold demonstrated in Guo et al. (2021). At the ~~global~~ Chinese soils scale, including samples from arid and humid environments, CBT' correlation is very strong with pH but not with MAP (Wang et al., 2019). It may show that the alkalinity effect on cyclisation is not enhanced by soil aridity but by other phenomena. In Guo et al. (2021) where pH and aridity are associated, the more arid conditions do not relate to increasing cyclisation number. Our results are in line with the study of Guo et al. (2021) who supports the use of IR_{6Me} for pH reconstruction. This consideration is important to keep in mind mainly for past brGDGT-based reconstructions carried out in shallow lake (with important soil influx) and loess-palaeosol sequences (Lin et al., 2024), since the effect on lacustrine samples is still unclear.

The IR outperforms the CBT for tracking pH because IR shows a single, consistent correlation with pH, whereas CBT .

4.2 Assessing confounding factors combined effects

Although temperature, both MAAT and MAF, remains a major bioclimate parameter controlling the brGDGT distribution, we have shown that other ~~confounding factors~~ environmental variables such as aridity and salinity are at least as important in explaining the brGDGT distribution from the ACADB. Particularly, ~~confounding factors~~ these variables do not only impact their related indices used as proxies (e.g., MAAT with MBT'_{5Me}, salinity with IR'_{6+7Me}, etc.) but also other indices (e.g., the ACA MBT'_{5Me} is also impacted by salinity). However, these ~~confounding~~ factors are typically studied independently, while in soil and lacustrine systems, multiple interacting factors complicate the understanding of their combined effects.

4.2.1 Combined effect of pH with other ~~confounding~~ controlling factors

Several complex interactions drive the pH effects on brGDGT assemblages. For example, pH is more related to the soil organic matter content than salinity in arid contexts (Muhammad et al., 2008), and in ACADB there is no correlation between pH and salinity for soil samples (Fig. 5). Similarly, humid environments are more likely to have organic-rich soil, influencing the pH (Liang et al., 2019). However, isomer ratios are influenced by both these physicochemical soil properties ~~.~~ (Fig. 8).

The alkalinity interaction with aridity has been already reported from Chinese brGDGT soil studies (Yang et al., 2014; Dang et al., 2016b). They show that the major brGDGT compounds are more diverse in arid than humid soils, implicating different correlations between brGDGT indices, pH, and MAAT for dry and for wet soils (Wang et al., 2019). Although the brGDGT cyclisation response to pH is globally well constrained, it is not the case in Chinese soils (Wang et al., 2019), but it is the case in northern Iran (Duan et al., 2022). Chen et al. (2021) introduced the use of soil water content as an intermediate parameter to clarify the pH-aridity interaction impact on brGDGT distribution. As a consequence, the brGDGT-based climate reconstructions of past archives in ACA need to be interpreted differently for alkaline samples.

4.2.2 Salinity effect and its relationship with aridity and sample types

The Procrustes rotation analysis performed on the ACADB reveals a different control of the environment on the brGDGT distribution from soil and from lacustrine origin. Particularly, in Fig. 5D and E, the salinity and AI were associated for lacustrine samples (i.e., the more humid the climate, the fresher the water), but surprisingly we observe the opposite association for soils. This could be due to the textural properties of soils, including the fact that salinization is more likely in clay than in sand (Muhammad et al., 2008). In this context, the numerous sandy desert samples in the ACADB from hyper-arid conditions do not have high salt content. For ACADB lacustrine samples, aridity enhances the salt water content, which is consistent with actual observations (Williams, 1999) as well as during the Holocene (So et al., 2023). The salinity effect on ~~not recalibrated~~ temperature reconstruction may result in a temperature over estimation of more than 2 °C (Liang et al., 2024). Although the salinity effect on 7-methyl compounds is more and more understood for lacustrine samples (Wang et al., 2021; Kou et al., 2022; So et al., 2023; Liang et al., 2024), it remains understudied for soil samples. We have shown that the ~~over-representativeness~~ average fractional abundance of 7-methyl brGDGTs is higher for lacustrine than soil samples. In soils, primarily the 6-methyl rather than the 5-methyl isomers seems to react to salinity, but this could be due to the combined effect of aridity, pH, and salinity. Salinity inferred by TDS is a bulk physicochemical parameter, and therefore, more details about the soil ionic composition are needed to refine the understanding of the salinity ~~confounding~~ controlling factor effect (Chen et al., 2022; De Jonge et al., 2024a).

4.2.3 Combined effects of climate aridity on soil moisture, pH, and its consequences on the brGDGT distribution

In the ACADB, it appears that aridity enhances the abundance of cyclised and 6-methyl compounds over Ia, IIa, and IIIa (Figs. 7 and 8). This effect of aridity on both isomerisation (i.e., favouring 6- over 5-methyls) and cyclisation (favouring compounds with high internal cyclisation number) is a well-known effect in Arid Central Asia, showing the complex interaction between arid climate conditions, soil moisture, and pH (Dang et al., 2016b; Chen et al., 2021). Since the aridity effect on brGDGT is not directly settled by precipitation (Wang et al., 2019) but rather by the soil water content (Sun et al., 2019; Chen et al., 2021), this could explain why the AI correlation with IR_{6Me} and CBT' is not as strong for lakes as it is for soils (in which aridity directly impacts soil water content). Soil water content shows a clear impact on arid environments from both Chinese (Dang et al., 2016b) and African (Loomis et al., 2011) soils. Since the soil water content is not a limiting factor for the bacterial community in soil, the diminution of oxygen content in soil may be responsible (Li et al., 2018). Liang et al. (2019) suggest that this

effect is particularly important in hyper- to semi-arid environments where bare soils (without vegetation cover) are dominant. In contrast, in humid environments, the important vegetation cover changes the soil organic content and, by extension, the soil pH. These physicochemical causal links could explain the aridity's combined effects on ACA brGDGT distribution.

4.2.4 Toward a ~~scale~~ ranking of ~~confounding~~ controlling factors ~~strength~~importance

~~Although several confounding factors~~ We have shown that brGDGT—environment relationships are influenced by several biases linked to confounding factors (Sect. 4.1; Figs. 5, 6, 7 and 8). In addition, interactions among these factors further limit proxy applicability (Sect. 4.2). A key next step to improve the reliability of brGDGTs as past environmental proxies is to rank the relative importance of these controlling influences. Although major environmental controlling factors have been identified ~~worldwide~~ globally (Naafs et al., 2017a; Dearing Crampton-Flood et al., 2020; Raberg et al., 2022a), ~~it seems that the dominance order of these biases is study dependent. At a~~ their dominance hierarchy appears to vary by study region and archive.

~~At the~~ global scale, temperature is ~~the primary factor~~consistently the primary control, followed by pH, ~~independent of the type of sample studied (Raberg et al., 2022a). However, the linear relationship between brGDGT indices and both MAAT and pH is sample type dependent (i.e., the linear slope and intercept are not similar for soil, peat and lacustrine samples, Naafs et al., 2017a, b)~~ regardless of sample type (Raberg et al., 2022a). This general ranking (temperature as primary factor and pH as secondary one) holds across environments, but sample type still modifies regression parameters: slopes and intercepts differ between soils, peats, and lake sediments (Naafs et al., 2017a, b). Then, ~~specific biases appear for specific sample types: mainly seasonality is important for lacustrine calibrations (Dang et al., 2018; Martínez-Sosa et al., 2021; Raberg et al., 2021). Even if seasonality also impacts soil-based~~ additional influences depend on specific sample type. For example, seasonal effects are strongest in lake-based calibrations (Dang et al., 2018; Martínez-Sosa et al., 2021; Raberg et al., 2021, 2022a). Seasonality also affects soil calibrations (Deng et al., 2016; Dearing Crampton-Flood et al., 2020), but it has been shown that the monthly temperature fluctuations reported by brGDGT indices were similar to the average temperature (Cao et al., 2018), mainly due to the slow turnover of brGDGT production and deposit in soil samples (Weijers et al., 2011). ~~In any case, seasonality is presented as one of the major confounding factors for global soil calibration (Dearing Crampton-Flood et al., 2020), while the aridity effect seems to be limited using Bayesian calibration.In brief, confounding factors studied at the global scale are slightly different from ones studied at~~ Overall, current evidence indicates that temperature and pH dominate brGDGT distributions, followed by sample type and proxy-specific modifiers such as seasonality, salinity, and aridity.

Our ACADB data suggest a different ranking of controlling factors for Arid Central Asia, and drylands more generally. Based on the MANOVA results (Table 3), salinity emerges as the dominant factor after temperature, followed by sample type, pH, and aridity, all contributing significantly to brGDGT variance. However, this ranking is derived from a limited subset of samples because salinity and pH measurements do not cover the entire dataset (Fig. 5). Moreover, the present approach is further limited by the *ex-situ* measurement of salinity and pH (Fig. 2). Ongoing microbial metabolic activity during sample transport and storage may have altered *in-situ* pH conditions prior to laboratory analysis, potentially biasing measured values. Nevertheless, the ACA ranking clearly differs from the global hierarchy. Previous regional and local ~~scales.~~

~~At the Chinese soil scale~~studies have likewise reported differences from the global-scale rankings. In Chinese soils, pH is the ~~dominant controlling factor on brGDGT distribution (even before temperature, Wang et al., 2019), while focused on~~ primary control on brGDGT distributions, surpassing temperature (Wang et al., 2019). In hyper- to semi-arid ~~environments, the~~ settings, annual precipitation and aridity become more ~~important than pH and~~ influential than either pH or temperature (Duan et al., 2022). ~~In their study, all soil samples from northern Iran are alkaline and characterized by high temperature; then the environmental gradient is controlled by the precipitation gradient instead of the pH or seasonality. In Iran, the extreme alkalinity conditions should be responsible for the difference in confounding factor dominance with global brGDGT studies. The seasonality bias on temperature is also climate dependent, with a stronger effect on areas with important seasonal variations, such as wide elevation gradients (Deng et al., 2016), continental areas, (Lei et al., 2016) and high latitudes (Dang et al., 2018; Ca~~ . ~~In contrast, seasonality effects are not reported from tropical area (Pérez-Angel et al., 2020; Häggi et al., 2023). From lacustrine samples from~~ For lacustrine archives on the Tibetan Plateau, salinity is the ~~first confounding~~ leading controlling factor (Liang et al., 2024). ~~The difference in~~ Such site-specific ~~confounding factors is supporting~~ variability in factor importance supports the idea that community ~~shift is more determinant~~ shifts, rather than physiological plasticity~~to explain the brGDGT response~~, primarily govern brGDGT responses to environmental parameters (Guo et al., 2021). This ~~idea is also supported by the observed threshold in the brGDGT calibration under different temperature conditions (De Jonge et al., 2019). However, physiological plasticity remains supported by simulations and incubation experiments (Naafs et al., 2021; Halamka et al., 2023). These considerations give another valuable argument to assess the local or regional scale of the confounding factor effect on brGDGT index applicability~~further underscores the need to evaluate controlling factors at local to regional scales when assessing the applicability of brGDGT-based indices.

4.3 brGDGT-based climate calibrations for drylands

~~We have shown that brGDGT-based indices are impacted in ACA by several confounding factors~~

4.3.1 Temperature calibration errors

As a result of the multiple controlling factors influencing the response of brGDGTs to climate, and their complex ~~interactions. Here, we discuss the possibility of applying and developing specific calibration for drylands, mainly focusing on specific combined effects,~~ traditional temperature calibrations exhibit substantial errors when cross-validated using the ACADB dataset (Fig. 10). This is true for both the Mean Annual Air Temperature (Fig. 10**A**) and the mean air temperature of Months Above Freezing (Fig. 10**B**). At the ACADB scale, local calibrations show a significant average bias, producing either overly warm (Yang et al., 2014; Sun et al., 2011; Thomas et al., 2017) or overly cold estimates (Wang et al., 2016). Although global calibrations reduce this offset, they still display wide dispersion (ranging from −20 to 35 °C). These large errors persist across various statistical approaches, including quadratic and multiple linear regressions, MBT'_{5Me}-based, and Bayesian calibrations. Altogether, these findings highlight the need for developing dedicated calibrations for dryland environments, particularly focusing on temperature and precipitation ~~calibrations for specific sample groups~~ reconstructions tailored to specific sample types (e.g., ~~fresh, hypersaline, etc.~~ freshwater vs. hypersaline systems).

4.3.2 Aridity and precipitation calibrations

The particular arid conditions in ACA have ~~constrained~~ led several studies to propose brGDGT-based precipitation reconstructions (mainly MAP) in parallel or instead of MAAT calibrations (Dugerdil et al., 2021a; Duan et al., 2022). In both cases, the statistical relationship between MBT'_{5Me} or MBT'_{6Me} matched precipitation better than temperature, and MR calibrations based on brGDGT fractional abundances were proposed. However, precipitation was inferred by MR calibration or cyclisation indices rather than by methylation indices (Dugerdil et al., 2021a; Duan et al., 2022). Moreover, even if no proper calibration is given, Lin et al. (2024) have shown a stronger linear correlation for MBT'_{5Me} with MAP than MAAT, especially for Chinese arid soils, giving specific interpretation for brGDGT loess-palaeosol sequences. A similar strong correlation with soil water content was also found in arid soils (Dang et al., 2016b).

4.3.3 brGDGT-temperature calibration

Our multivariate (Fig. 5) and univariate (Figs. 6 and ~~11~~8) results have shown that several confounding factors can at least influence or at worst reverse the palaeothermometer calibration trends in drylands. The results of analyses of variance particularly evidence the influence of salinity and sample type on brGDGT FA. Mixing soil and lacustrine samples for such calibration raises the risk of misleading correlations. In ACA, MBT'_{5Me}-based palaeothermometer should be applied carefully or, even better, it should be recalibrated by confounding factor classes. Mainly, the ACADB analysis of variance carried out on several brGDGT indices reveals that the *sample type* effect is weaker than salinity and as strong as pH. If the *sample type* effect is already leading to particular calibration (i.e., soil, peat, and lacustrine ones) in global (De Jonge et al., 2014; Naafs et al., 2017a, b; Dearing Crampton-Flood et al., 2020; Martínez-Sosa et al., 2021) and regional calibrations (Sun et al., 2011; Yang et al., 2014; Chen et al., 2021), leading to specific peat, lake, and soil calibrations, caution needs to be taken with sample type calibrations in drylands. This is because, first, the *sample type* information for each sample is not always an indisputable observation. Lacustrine samples can be undoubtedly determined only from a deep lake (which is rare in drylands). Most ACA lakes from the lowland basin are temporary ponds, seasonally drained, while several soil samples come from *solonchak* (i.e., saline rangelands covered by halophytic vegetation and periodically flooded, Gintzburger, 2003). For high-elevation lakes, due to their low level of water, the amount of soil influx from water springs and aerial dust is important. They also commonly have a semi-peatland behaviour due to the hydrophytic vegetation colonisation from belt to lake centre in the context of shallow water level (Cromartie et al., 2020; Robles et al., 2022). Among the difficulties encountered in reconstructing accurate temperatures with brGDGT, the temperature offset between global calibration and study site climate context appears. In most cases, MAAT or MAF inferred by brGDGT shows an important shift between actual MAAT and reconstructed MAAT for the lacustrine ~~top cores~~ core tops (Martin et al., 2019; Dugerdil et al., 2021b; d'Oliveira et al., 2023). Using a local ~~calibration (Dugerdil et al., 2021a) or locally recalibrated global calibration (Chen et al., 2021)~~ or regional calibration (Dugerdil et al., 2021a; Chen et al., 2021), generally reduces this offset. Comparing pollen-based and brGDGT-based temperatures also reveals that the brGDGT-MAAT relationship has wider temperature variation over the same time span (Robles et al., 2022; d'Oliveira et al., 2023).

4.3.4 Confounding factors effect on temperature calibrations

While $\text{MBT}'_{5\text{Me}}$-based temperature calibrations are commonly specified only based on the sample type (i.e., separate calibrations exist for soil, peat, and lacustrine samples), we have shown previously that the statistically most influential confounding factor in the ACADB was salinity before pH and sample type. Mainly, the Procrustes rotation analyses show similar multivariate spaces for soil and lacustrine samples (Fig. 5C and F). Based on this finding, specific calibrations based on salinity classes are tested on Fig. 11. The same tests were applied for pH (Fig. S.7), aridity (Fig. S.8) and sample type (Fig. S.9).

~~For the salinity classes , all except adjusted-regression hyposaline are improved compared to the global regression~~ Salinity classes were based on a classification adapted from (Rusydi, 2018). The TDS cut-offs were refined using sensitivity analysis and are reported in Table S.3. In Fig. S.7, all adjusted regressions – except for hyposaline samples – perform better than the global model (i.e., the full ACADB), ~~especially for fresh water, hypersalineand saline~~ with the largest improvements for freshwater, hypersaline, and saline samples (R^2_{adj} of 0.61, 0.49, and 0.37, respectively). This method principally improves the statistical result for extreme classes. However, this improvement could be artificial and only produced by statistical biases such as the dataset size or the reduction of variance among groups. To ensure relevant salinity-specific calibrations, the z-statistic checks differences between regressions. Fresh calibration has a different slope than hyposaline and the whole dataset with z(a) = 2.7*** and 2.5***. Saline samples share a similar slope with hyposaline but a different offset with z(b) = -2.2**. No conclusion can be made for hypersaline due to high variance. Saline and likely hypersaline have a similar slope to hyposaline but a significantly higher offset (z(b) = -2.8*** with hyposaline, z(b) = 2.3*** with the whole dataset). This analysis allows for ACA $\text{MBT}'_{5\text{Me}}$ calibration based on salinity classes [Eq. (6)].

$$\text{MAAT}_{\text{Fresh}} = -6.37 + 28.03 \times \text{MBT}'_{5\text{Me}}, (n = 61, R^2_{\text{adj}} = 0.61, \text{RMSE} = 4)$$

$$\text{MAAT}_{\text{Sal.}} = -11.1 + 23.17 \times \text{MBT}'_{5\text{Me}} (n = 45, R^2_{\text{adj}} = 0.32, \text{RMSE} = 5.22)$$

$$\text{MAAT}_{\text{Hypersal.}} = -8.33 + 22.36 \times \text{MBT}'_{5\text{Me}} (n = 17, R^2_{\text{adj}} = 0.47, \text{RMSE} = 3.88)$$

All the linear models in Eq. (6) have a p-value < 0.001 when tested using 20,000-permutation significance tests.

$$\text{MAAT}_{\text{Fresh}} = -6.37 + 28.03 \times \text{MBT}'_{5\text{Me}}, (n = 61, R^2_{\text{adj}} = 0.61, \text{RMSE} = 4) \tag{6.1}$$

$$\text{MAAT}_{\text{Hyposal.}} = -3.87 + 16.72 \times \text{MBT}'_{5\text{Me}}, (n = 215, R^2_{\text{adj}} = 0.12, \text{RMSE} = 5.97) \tag{6.2}$$

$$\text{MAAT}_{\text{Sal.}} = -11.1 + 23.17 \times \text{MBT}'_{5\text{Me}}, (n = 45, R^2_{\text{adj}} = 0.32, \text{RMSE} = 5.22) \tag{6.3}$$

$$\text{MAAT}_{\text{Hypersal.}} = -8.33 + 22.36 \times \text{MBT}'_{5\text{Me}}, (n = 17, R^2_{\text{adj}} = 0.47, \text{RMSE} = 3.88) \tag{6.4}$$

$$\text{MAAT}_{\text{All}} = -6.28 + 20.19 \times \text{MBT}'_{5\text{Me}}, (n = 761, R^2_{\text{adj}} = 0.27, \text{RMSE} = 5.62) \tag{6.5}$$

4.4 Recommendations for brGDGT applications to past records in drylands

4.4.1 Differential brGDGT sources effect in the past

~~If one of the solutions to reduce biases for~~ Developing calibrations for specific sediment types can help reduce biases in brGDGT-based climate reconstructions~~in the past is to lead *sediment type* particular brGDGT calibrations, some tricky issues~~, but some challenges remain. (1) The sediment type characterisation has to be reliable. Several studies attempt to use brGDGT themselves as a proxy of brGDGT sources based on mixing models (Martin et al., 2019) or classification machine learning approaches (Martínez-Sosa et al., 2023; Cromartie et al., 2025). Other proxies of the sample type could be a more reliable solution to evaluate the environmental condition of brGDGT deposit (Robles et al., 2022; d'Oliveira et al., 2023). (2) The brGDGT influx is not always related to the sediment deposit flux itself. In some particular conditions, a lake can record soil-produced brGDGT coming from the watershed instead of *in-situ* produced brGDGT (Zhao et al., 2021; Robles et al., 2022). In some other conditions, the *in-situ* production is dominant in the brGDGT assemblage (Wang et al., 2021; Kou et al., 2022). (3) When sediment types vary along a core, accurately characterizing them becomes challenging, making it difficult to apply a single brGDGT-based climate calibration. For instance, using a uniform lacustrine calibration may yield inconsistent results when applied to both hypersaline and freshwater lake samples, as illustrated in Fig. 11.

4.4.2 Confounding impacts and correction in the past

Then, the past sediment type characterisation appears to be insufficient to reliably apply selective brGDGT-based climate calibrations. The main confounding factor effect has to be taken into account. However, these confounding factors are study-context dependent: the saturation effect of the $\mathrm{MBT'_{5Me}}$ and the vegetation buffer in tropical areas (Pérez-Angel et al., 2020; Häggi et al., 2023), the important seasonality in the Arctic (Raberg et al., 2021), soil moisture and salinity impact in drylands (Fig. 11; Dang et al., 2016b; Kou et al., 2022), etc. A second limitation of this grouping factor selective calibration approach in the past is that the confounding factor impact is not always stationary over time. For instance, salinity (So et al., 2023) or vegetation cover (Robles et al., 2022; d'Oliveira et al., 2023) dramatically shifted in the past. It is particularly the case during the Holocene in ACA (Chen et al., 2024). In this case, inferring confounding factor covariation has to be considered. Several studies attempt to track these covariations using brGDGT-based confounding factor proxies, such as isomer ratios (Liang et al., 2024). Some others use a multi-proxy approach (e.g., pollen or chironomids) to independently infer the confounding factor variation trends (Dugerdil et al., 2021a, b; Robles et al., 2022; d'Oliveira et al., 2023).

To improve the regression between $\mathrm{MBT'5Me}$ and MAAT, we apply calibrations using different grouping factors, mainly salinity (Wang et al., 2021, Fig. 11), but also pH and aridity (Figs. S.7 and S.8). Chen et al. (2021) split the GDGT dataset by surface sample pH (threshold of pH = 7), which is reflected in the ACADB CBT'-pH relationship (Fig. 7A and B) and reported in arid soils (Guo et al., 2021). Similarly, Wang et al. (2021) improved the $\mathrm{MBT'5Me}$-based temperature calibration for Tibetan lacustrine samples by including salinity, but quantitative values for these factors are unavailable for past brGDGT sequences.

One of the solutions to fulfil this lack of information about the deposit system in the past is to make differential calibrations not on confounding factor values but on brGDGT-based proxies of these confounding factor values. Such an approach has been tested in Véquaud et al. (2022), using the Community Index (De Jonge et al., 2019) with ~~mitigated~~ limited regression improvement. In Véquaud et al. (2022), the two clusters based on the Community Index threshold were thought to improve the temperature reconstruction by showing specific regression for each of them. However, the two sub-groups give mitigated determination coefficient (R^2 of 0.20 and 0.71). More recently, Liang et al. (2024) propose to use the isomer ratio (since this index includes both salinity and pH effects) to constrain $\mathrm{MBT'_{5Me}}$-based MAAT calibration with more reliable results in saline lakes. All these attempts are still incomplete to totally correct the brGDGT-based temperature reconstruction bias, even if they significantly reduce the over-estimation of MAAT. In any case, a careful examination of the brGDGT distribution from past archives is essential to minimize errors resulting from the inappropriate selection of applied calibrations.

5   Conclusions

The brGDGT-based palaeothermometer is one of the most promising approaches to improve our understanding of past climate in different regions of the world. However, based on the comparison between an ACA-centred database and the world surface sample database, our study has shown that:

1. Drylands suffer from particular climate and physicochemical properties of soils and lakes, enhancing the impact of confounding factors on brGDGT-based $\mathrm{MBT'_{5Me}}$ and fractional abundances' relationship with MAAT.

2. Among the ~~confounding~~ controlling factors (i.e., pH, aridity, salinity, and sample type), salinity is the most dominant, followed by sample type and pH. However, aridity plays a major role in the brGDGT variance among the dataset. Moreover, these biases cannot be studied individually since their interactions are not always similar. For instance, the salinity control on brGDGT isomerisation is different in soil and lacustrine deposit contexts.

3. In order to use brGDGT as a proxy for sediment physicochemical conditions, it appears that the $\mathrm{IR'_{6+7Me}}$ is the best index of salinity, while $\mathrm{IR_{6Me}}$ is the best for pH reconstruction despite its saturation effect for pH < 4 and pH > 10. For aridity, drawing $\Delta(\mathrm{MBT'_{5Me}}, \mathrm{MBT'_{6Me}})$ gives a fairly reliable estimate.

4. $\mathrm{MBT'_{5Me}}$ relationship with MAAT is very limited in ACA, especially for lacustrine samples, mitigating the applicability of palaeothermometers based on methylation indices. However, the specific sub-calibrations for different environmental classes (mainly salinity and aridity classes) dramatically improve the linear regression strength. This report paves the way for a specific calibration application on past brGDGT sequences based on environmental classes inferred or by brGDGT indices or by other independent proxies (e.g., pollen or chironomids).

Mainly, even if the brGDGT signal in drylands such as ACA is mitigated and the number of ~~confounding~~ controlling factors is sometimes difficult to unravel, it remains a very promising tool to improve our understanding of both past climate and future forecasting (Tierney et al., 2020). However, some work still remains in process, including the increase of arid sites in

the database (both for the calibration process associated with exhaustive physicochemical and bioclimatic properties of the samples and for the past brGDGT sequences enhanced by a multi-proxy approach) and the development of a machine learning approach, which promises a more powerful unravelling process of ~~confounding~~ controlling factor comprehension.

Code availability. The R scripts used to clean, analysed the ACADB surface brGDGT data and plot all the figures presented in this study (except Fig. 1 and 2 realized in `QGIS` and `Inkscape`) are open and available on the following GitHub repository: https://github.com/LucasDugerdil/GDGT_ACADB/.

Data availability. Sample location and features, brGDGT fractional abundances and concentrations, brGDGT-based indices, bioclimate, and physicochemical parameters are available on PANGAEA dataset XXXX.

Author contributions. *Conceptualization*: LD, SJ, OP, MG; *Data curation*: LD; *Formal analysis*: LD, AC, GM, SAA; *Funding acquisition*: SJ, XH, BB, FC, GM; *Investigation*: LD, SB, XH, JA, RS, IM, SI, SM, EA, SI, PG; *Methodology*: LD, SJ, OP, MG; *Project administration*: LD, SJ, OP, MG; *Resources*: LD, SB, XH, FC, DE, JA, BB, JH, LS, KM, RS, IM, SI, SM, EA, SI, PG; *Software*: LD, AC; *Supervision*: LD, SJ, OP, MG; *Validation*: LD, SJ, OP, MG, XH, FC, BB; *Visualization*: LD; *Writing – original draft*: LD; *Writing – review & editing*: all authors.

Competing interests. The authors declare that they have no known competing financial interests or personal relationships that could have appeared to influence the work reported in this paper.

Acknowledgements. This research was funded, in whole or in part, by ANR, Grant ANR-22-CE27-0018-02, and Grant ANR-20-FRAL-0006. The ENS de Lyon financed the PhD scholarship of L. Dugerdil. We are grateful to *La Tendresse*, Sarah Millet-Amrani, and Zoé Hernandez for their valuable support in France; Nozimbek Namozovich and Sokhib Abdusamatov in Uzbekistan; and Gulmirzozoda Masnavi Gulmirzo in Tajikistan. We are grateful to Vivien Mai Yung Sen for his help in high mountain sampling in Hissar and Pamir. Thanks to Elodie Brisset (IMBE) and Johanna Lhuillier (Archéorient) for their support during the Uzbekistan field trips. Bazartseren Boldgiv is supported by the Taylor Family-Asia Foundation Endowed Chair in Ecology and Conservation Biology. This is an ISEM contribution XXXX.

References

Baxter, A. J., Hopmans, E. C., Russell, J. M., and Sinninghe Damsté, J. S.: Bacterial GMGTs in East African Lake Sediments: Their Potential as Palaeotemperature Indicators, Geochimica et Cosmochimica Acta, 259, 155–169, https://doi.org/10.1016/j.gca.2019.05.039, 2019.

Bierens, H. J.: Uniform Consistency of Kernel Estimators of a Regression Function under Generalized Conditions, Journal of the American Statistical Association, 78, 699–707, https://doi.org/10.1080/01621459.1983.10478031, 1983.

Bivand, R., Keitt, T., Rowlingson, B., Pebesma, E., Sumner, M., Hijmans, R., Rouault, E., and Bivand, M. R.: Package 'Rgdal', Bindings for the Geospatial Data Abstraction Library. Available online: https://cran. r-project. org/web/packages/rgdal/index. html (accessed on 15 October 2017), 172, 2015.

Bunting, M., Farrell, M., Broström, A., Hjelle, K., Mazier, F., Middleton, R., Nielsen, A., Rushton, E., Shaw, H., and Twiddle, C.: Palynological Perspectives on Vegetation Survey: A Critical Step for Model-Based Reconstruction of Quaternary Land Cover, Quaternary Science Reviews, 82, 41–55, https://doi.org/10.1016/j.quascirev.2013.10.006, 2013.

Cao, M., Rueda, G., Rivas-Ruiz, P., Trapote, M. C., Henriksen, M., Vegas-Vilarrúbia, T., and Rosell-Melé, A.: Branched GDGT Variability in Sediments and Soils from Catchments with Marked Temperature Seasonality, Organic Geochemistry, 122, 98–114, https://doi.org/10.1016/j.orggeochem.2018.05.007, 2018.

Cao, X.-y., Herzschuh, U., Telford, R. J., and Ni, J.: A Modern Pollen–Climate Dataset from China and Mongolia: Assessing Its Potential for Climate Reconstruction, Review of Palaeobotany and Palynology, 211, 87–96, https://doi.org/10.1016/j.revpalbo.2014.08.007, 2014.

Chen, C., Bai, Y., Fang, X., Zhuang, G., Khodzhiev, A., Bai, X., and Murodov, A.: Evaluating the Potential of Soil Bacterial Tetraether Proxies in Westerlies Dominating Western Pamirs, Tajikistan and Implications for Paleoenvironmental Reconstructions, Chemical Geology, 559, 119 908, https://doi.org/10.1016/j.chemgeo.2020.119908, 2021.

Chen, S., Chen, J., Ding, G., Ma, S., Ji, P., Zhou, A., Wu, D., Khormali, F., Hou, J., and Chen, F.: Dipole Pattern of Holocene Hydroclimate Variations across the Asian Drylands: Critical Evidence from West Asia, Journal of Geophysical Research: Atmospheres, 129, e2023JD039 413, https://doi.org/10.1029/2023JD039413, 2024.

Chen, Y., Zhang, X., Qi, W., Zhang, G., Pei, Y., Fang, X., Xia, Y., and Zhang, S.: Distribution of Glycerol Dialkyl Glycerol Tetraethers (GDGTs) in Carbonate-Type and Sulfate-Type Lacustrine Sediments: Insight into the Influence of Ionic Composition on GDGTs, Minerals, 12, 1233, https://doi.org/10.3390/min12101233, 2022.

Clogg, C. C., Petkova, E., and Haritou, A.: Statistical Methods for Comparing Regression Coefficients between Models, American Journal Of Sociology, 100, 1261–1293, https://doi.org/10.1086/230638, 1995.

Cromartie, A., Blanchet, C., Barhoumi, C., Messager, E., Peyron, O., Ollivier, V., Sabatier, P., Etienne, D., Karakhanyan, A., Khatchadourian, L., Smith, A. T., Badalyan, R., Perello, B., Lindsay, I., and Joannin, S.: The Vegetation, Climate, and Fire History of a Mountain Steppe: A Holocene Reconstruction from the South Caucasus, Shenkani, Armenia, Quaternary Science Reviews, 246, 106 485, https://doi.org/10.1016/j.quascirev.2020.106485, 2020.

Cromartie, A., De Jonge, C., Ménot, G., Robles, M., Dugerdil, L., Peyron, O., Rodrigo-Gámiz, M., Camuera, J., Ramos-Roman, M. J., Jiménez-Moreno, G., Colombié, C., Sahakyan, L., and Joannin, S.: Utilizing Probability Estimates from Machine Learning and Pollen to Understand the Depositional Influences on Branched GDGT in Wetlands, Peatlands, and Lakes, https://doi.org/10.5194/egusphere-2025-526, 2025.

Dang, X., Xue, J., Yang, H., and Xie, S.: Environmental Impacts on the Distribution of Microbial Tetraether Lipids in Chinese Lakes with Contrasting pH: Implications for Lacustrine Paleoenvironmental Reconstructions, Science China Earth Sciences, 59, 939–950, https://doi.org/10.1007/s11430-015-5234-z, 2016a.

Dang, X., Yang, H., Naafs, B. D. A., Pancost, R. D., and Xie, S.: Evidence of Moisture Control on the Methylation of Branched Glycerol Dialkyl Glycerol Tetraethers in Semi-Arid and Arid Soils, Geochimica et Cosmochimica Acta, 189, 24–36, https://doi.org/10.1016/j.gca.2016.06.004, 2016b.

Dang, X., Ding, W., Yang, H., Pancost, R. D., Naafs, B. D. A., Xue, J., Lin, X., Lu, J., and Xie, S.: Different Temperature Dependence of the Bacterial brGDGT Isomers in 35 Chinese Lake Sediments Compared to That in Soils, Organic Geochemistry, 119, 72–79, https://doi.org/10/gdfs3x, 2018.

Davtian, N., Bard, E., Ménot, G., and Fagault, Y.: The Importance of Mass Accuracy in Selected Ion Monitoring Analysis of Branched and Isoprenoid Tetraethers, Organic geochemistry, 118, 58–62, https://doi.org/10/gdc8rs, 2018.

De Jonge, C., Hopmans, E. C., Zell, C. I., Kim, J.-H., Schouten, S., and Sinninghe Damsté, J. S.: Occurrence and Abundance of 6-Methyl Branched Glycerol Dialkyl Glycerol Tetraethers in Soils: Implications for Palaeoclimate Reconstruction, Geochimica et Cosmochimica Acta, 141, 97–112, https://doi.org/10/f6h2xw, 2014.

De Jonge, C., Stadnitskaia, A., Fedotov, A., and Sinninghe Damsté, J. S.: Impact of Riverine Suspended Particulate Matter on the Branched Glycerol Dialkyl Glycerol Tetraether Composition of Lakes: The Outflow of the Selenga River in Lake Baikal (Russia), Organic Geochemistry, 83–84, 241–252, https://doi.org/10.1016/j.orggeochem.2015.04.004, 2015.

De Jonge, C., Radujković, D., Sigurdsson, B. D., Weedon, J. T., Janssens, I., and Peterse, F.: Lipid Biomarker Temperature Proxy Responds to Abrupt Shift in the Bacterial Community Composition in Geothermally Heated Soils, Organic Geochemistry, 137, 103 897, https://doi.org/10.1016/j.orggeochem.2019.07.006, 2019.

De Jonge, C., Guo, J., Hällberg, P., Griepentrog, M., Rifai, H., Richter, A., Ramirez, E., Zhang, X., Smittenberg, R. H., and Peterse, F.: The Impact of Soil Chemistry, Moisture and Temperature on Branched and Isoprenoid GDGTs in Soils: A Study Using Six Globally Distributed Elevation Transects, Organic Geochemistry, 187, 104 706, https://doi.org/10.1016/j.orggeochem.2023.104706, 2024a.

De Jonge, C., Peterse, F., Nierop, K. G. J., Blattmann, T. M., Alexandre, M., Ansanay-Alex, S., Austin, T., Babin, M., Bard, E., Bauersachs, T., Blewett, J., Boehman, B., Castañeda, I. S., Chen, J., Conti, M. L. G., Contreras, S., Cordes, J., Davtian, N., Van Dongen, B., Duncan, B., Elling, F. J., Galy, V., Gao, S., Hefter, J., Hinrichs, K.-U., Helling, M. R., Hoorweg, M., Hopmans, E., Hou, J., Huang, Y., Huguet, A., Jia, G., Karger, C., Keely, B. J., Kusch, S., Li, H., Liang, J., Lipp, J. S., Liu, W., Lu, H., Mangelsdorf, K., Manners, H., Martinez Garcia, A., Menot, G., Mollenhauer, G., Naafs, B. D. A., Naeher, S., O'Connor, L. K., Pearce, E. M., Pearson, A., Rao, Z., Rodrigo-Gámiz, M., Rosendahl, C., Rostek, F., Bao, R., Sanyal, P., Schubotz, F., Scott, W., Sen, R., Sluijs, A., Smittenberg, R., Stefanescu, I., Sun, J., Sutton, P., Tierney, J., Tejos, E., Villanueva, J., Wang, H., Werne, J., Yamamoto, M., Yang, H., and Zhou, A.: Interlaboratory Comparison of Branched GDGT Temperature and pH Proxies Using Soils and Lipid Extracts, Geochemistry, Geophysics, Geosystems, 25, e2024GC011 583, https://doi.org/10.1029/2024GC011583, 2024b.

Dearing Crampton-Flood, E., Tierney, J. E., Peterse, F., Kirkels, F. M. S. A., and Sinninghe Damsté, J. S.: BayMBT: A Bayesian Calibration Model for Branched Glycerol Dialkyl Glycerol Tetraethers in Soils and Peats, Geochimica et Cosmochimica Acta, 268, 142–159, https://doi.org/10/gg9758, 2020.

Deng, L., Jia, G., Jin, C., and Li, S.: Warm Season Bias of Branched GDGT Temperature Estimates Causes Underestimation of Altitudinal Lapse Rate, Organic Geochemistry, 96, 11–17, https://doi.org/10.1016/j.orggeochem.2016.03.004, 2016.

Ding, S., Schwab, V. F., Ueberschaar, N., Roth, V.-N., Lange, M., Xu, Y., Gleixner, G., and Pohnert, G.: Identification of Novel 7-Methyl and Cyclopentanyl Branched Glycerol Dialkyl Glycerol Tetraethers in Lake Sediments, Organic Geochemistry, 102, 52–58, https://doi.org/10/f9mmqv, 2016.

Dixon, P.: VEGAN, a Package of R Functions for Community Ecology, Journal of Vegetation Science, 14, 927–930, https://doi.org/10/dz9txb, 2003.

d'Oliveira, L., Dugerdil, L., Ménot, G., Evin, A., Muller, S. D., Ansanay-Alex, S., Azuara, J., Bonnet, C., Bremond, L., Shah, M., and Peyron, O.: Reconstructing 15 000 Years of Southern France Temperatures from Coupled Pollen and Molecular (Branched Glycerol Dialkyl Glycerol Tetraether) Markers (Canroute, Massif Central), Climate of the Past, 19, 2127–2156, https://doi.org/10.5194/cp-19-2127-2023, 2023.

Duan, Y., Sun, Q., Werne, J. P., Yang, H., Jia, J., Wang, L., Xie, H., and Chen, F.: Soil pH Dominates the Distributions of Both 5- and 6-Methyl Branched Tetraethers in Arid Regions, Journal of Geophysical Research: Biogeosciences, 125, e2019JG005 356, https://doi.org/10.1029/2019jg005356, 2020.

Duan, Y., Sun, Q., Werne, J. P., Hou, J., Yang, H., Wang, Q., Khormali, F., and Chen, F.: The Impact of Precipitation on the Distributions of Branched Tetraethers in Alkaline Soils, Organic Geochemistry, 169, 104 410, https://doi.org/10.1016/j.orggeochem.2022.104410, 2022.

Dugerdil, L., Joannin, S., Peyron, O., Jouffroy-Bapicot, I., Vannière, B., Boldgiv, B., Unkelbach, J., Behling, H., and Ménot, G.: Climate Reconstructions Based on GDGT and Pollen Surface Datasets from Mongolia and Baikal Area: Calibrations and Applicability to Extremely Cold–Dry Environments over the Late Holocene, Climate of the Past, 17, 1199–1226, https://doi.org/10.5194/cp-17-1199-2021, 2021a.

Dugerdil, L., Ménot, G., Peyron, O., Jouffroy-Bapicot, I., Ansanay-Alex, S., Antheaume, I., Behling, H., Boldgiv, B., Develle, A.-L., Grossi, V., Magail, J., Makou, M., Robles, M., Unkelbach, J., Vannière, B., and Joannin, S.: Late Holocene Mongolian Climate and Environment Reconstructions from brGDGTs, NPPs and Pollen Transfer Functions for Lake Ayrag: Paleoclimate Implications for Arid Central Asia, Quaternary Science Reviews, 273, 107 235, https://doi.org/10.1016/j.quascirev.2021.107235, 2021b.

Dugerdil, L., Joannin, S., Peyron, O., Cromartie, A., Robles, M., Duan, Y., Huang, X., Chen, F., and Ménot, G.: Boosted Regression Trees Machine Learning Method Improves the brGDGT-based Climate Reconstruction in Drylands, Paleoceanography and Paleoclimatology, 40, e2025PA005 214, https://doi.org/10.1029/2025PA005214, 2025a.

Dugerdil, L., Peyron, O., Ménot, G., Egamberdieva, D., Alimov, J., Leroy, S. A., Garnier, E., Nowak, A., and Joannin, S.: First Paleoenvironmental Calibrations for Modern Pollen Rain of Tajikistan and Uzbekistan: A Case Study of Pollen - Vegetation Functional Biogeography of Arid Central Asia, Global and Planetary Change, p. 104857, https://doi.org/10.1016/j.gloplacha.2025.104857, 2025b.

Fick, S. E. and Hijmans, R. J.: WorldClim 2: New 1-Km Spatial Resolution Climate Surfaces for Global Land Areas: NEW CLIMATE SURFACES FOR GLOBAL LAND AREAS, International Journal of Climatology, 37, 4302–4315, https://doi.org/10/gb2jnq, 2017.

Gintzburger, G.: Rangelands of the Arid and Semi-Arid Zones in Uzbekistan, Editions Quae, 2003.

Guo, J., Ma, T., Liu, N., Zhang, X., Hu, H., Ma, W., Wang, Z., Feng, X., and Peterse, F.: Soil pH and Aridity Influence Distributions of Branched Tetraether Lipids in Grassland Soils along an Aridity Transect, Organic Geochemistry, 164, 104 347, https://doi.org/10.1016/j.orggeochem.2021.104347, 2021.

Häggi, C., Naafs, B. D. A., Silvestro, D., Bertassoli, D. J., Akabane, T. K., Mendes, V. R., Sawakuchi, A. O., Chiessi, C. M., Jaramillo, C. A., and Feakins, S. J.: GDGT Distribution in Tropical Soils and Its Potential as a Terrestrial Paleothermometer Revealed by Bayesian Deep-Learning Models, Geochimica et Cosmochimica Acta, https://doi.org/10.1016/j.gca.2023.09.014, 2023.

Halamka, T. A., Raberg, J. H., McFarlin, J. M., Younkin, A. D., Mulligan, C., Liu, X.-L., and Kopf, S. H.: Production of Diverse brGDGTs by Acidobacterium Solibacter Usitatus in Response to Temperature, pH, and O2 Provides a Culturing Perspective on Br GDGT Proxies and Biosynthesis, Geobiology, 21, 102–118, https://doi.org/10.1111/gbi.12525, 2023.

Hällberg, P. L., Smittenberg, R., Kylander, M. E., Villanueva, J., Davtian, N., Hapsari, A., Sjöström, J. K., Axelsson, J., Jarne-Bueno, G., Yamoah, K., Rifai, H., and Schenk, F.: Disentangling Seasonal and Annual Precipitation Signals in the Tropics over the Holocene: Insights from δD, Alkanes and GDGTs, Quaternary Science Reviews, 344, 108 948, https://doi.org/10.1016/j.quascirev.2024.108948, 2024.

Hamilton, N. and Ferry, M.: Ggtern : Ternary Diagrams Using Ggplot2, Journal of statistical software, 87, 1, https://doi.org/10.18637/jss.v087.c03, 2018.

Hijmans, R. J., Van Etten, J., Cheng, J., Mattiuzzi, M., Sumner, M., Greenberg, J. A., Lamigueiro, O. P., Bevan, A., Racine, E. B., and Shortridge, A.: Package 'Raster', R package, 734, 473, 2015.

Huguet, C., Hopmans, E. C., Febo-Ayala, W., Thompson, D. H., Sinninghe Damsté, J. S., and Schouten, S.: An Improved Method to Determine the Absolute Abundance of Glycerol Dibiphytanyl Glycerol Tetraether Lipids, Organic Geochemistry, 37, 1036–1041, https://doi.org/10.1016/j.orggeochem.2006.05.008, 2006.

Jarvis, A., Guevara, E., Reuter, H., and Nelson, A.: Hole-Filled SRTM for the Globe : Version 4 : Data Grid, 2008.

Khodzher, T. V., Domysheva, V. M., Sorokovikova, L. M., Sakirko, M. V., and Tomberg, I. V.: Current Chemical Composition of Lake Baikal Water, Inland Waters, 7, 250–258, https://doi.org/10.1080/20442041.2017.1329982, 2017.

Kou, Q., Zhu, L., Ju, J., Wang, J., Xu, T., Li, C., and Ma, Q.: Influence of Salinity on Glycerol Dialkyl Glycerol Tetraether-Based Indicators in Tibetan Plateau Lakes: Implications for Paleotemperature and Paleosalinity Reconstructions, Palaeogeography, Palaeoclimatology, Palaeoecology, 601, 111 127, https://doi.org/10.1016/j.palaeo.2022.111127, 2022.

Lei, Y., Yang, H., Dang, X., Zhao, S., and Xie, S.: Absence of a Significant Bias towards Summer Temperature in Branched Tetraether-Based Paleothermometer at Two Soil Sites with Contrasting Temperature Seasonality, Organic Geochemistry, 94, 83–94, https://doi.org/10.1016/j.orggeochem.2016.02.003, 2016.

Leroy, S. A., Kakroodi, A. A., Kroonenberg, S., Lahijani, H. K., Alimohammadian, H., and Nigarov, A.: Holocene Vegetation History and Sea Level Changes in the SE Corner of the Caspian Sea: Relevance to SW Asia Climate, Quaternary Science Reviews, 70, 28–47, https://doi.org/10.1016/j.quascirev.2013.03.004, 2013.

Li, J., Naafs, B. D. A., Pancost, R. D., Yang, H., Liu, D., and Xie, S.: Distribution of Branched Tetraether Lipids in Ponds from Inner Mongolia, NE China: Insight into the Source of brGDGTs, Organic Geochemistry, 112, 127–136, https://doi.org/10.1016/j.orggeochem.2017.07.005, 2017.

Li, Y., Zhao, S., Pei, H., Qian, S., Zang, J., Dang, X., and Yang, H.: Distribution of Glycerol Dialkyl Glycerol Tetraethers in Surface Soils along an Altitudinal Transect at Cold and Humid Mountain Changbai: Implications for the Reconstruction of Paleoaltimetry and Paleoclimate, Science China Earth Sciences, 61, 925–939, https://doi.org/10.1007/s11430-017-9168-9, 2018.

Liang, J., Russell, J. M., Xie, H., Lupien, R. L., Si, G., Wang, J., Hou, J., and Zhang, G.: Vegetation Effects on Temperature Calibrations of Branched Glycerol Dialkyl Glycerol Tetraether (brGDGTs) in Soils, Organic Geochemistry, 127, 1–11, https://doi.org/10.1016/j.orggeochem.2018.10.010, 2019.

Liang, J., Chevalier, M., Liu, K., Perfumo, A., Wang, M., Xie, H., Hou, J., Herzschuh, U., and Chen, F.: Discrepancies in Lacustrine Bacterial Lipid Temperature Reconstructions Explained by Microbial Ecology, Communications Earth & Environment, 5, 1–14, https://doi.org/10.1038/s43247-024-01925-3, 2024.

Lin, T., Rao, Z., Zeng, Y., Li, Y., Zhao, L., Liu, L., Xiao, X., Zhang, C., Shen, Z., Cao, J., and Jia, G.: Sedimentary brGDGTs in China: An Overview of Modern Observations and Proposed Land Holocene Paleotemperature Records, Earth-Science Reviews, 250, 104 694, https://doi.org/10.1016/j.earscirev.2024.104694, 2024.

Loomis, S. E., Russell, J. M., and Sinninghe Damsté, J. S.: Distributions of Branched GDGTs in Soils and Lake Sediments from Western Uganda: Implications for a Lacustrine Paleothermometer, Organic Geochemistry, 42, 739–751, https://doi.org/10.1016/j.orggeochem.2011.06.004, 2011.

Maestre, F. T., Le Bagousse-Pinguet, Y., Delgado-Baquerizo, M., Eldridge, D. J., Saiz, H., Berdugo, M., Gozalo, B., Ochoa, V., Guirado, E., García-Gómez, M., Valencia, E., Gaitán, J. J., Asensio, S., Mendoza, B. J., Plaza, C., Díaz-Martínez, P., Rey, A., Hu, H.-W., He, J.-Z., Wang, J.-T., Lehmann, A., Rillig, M. C., Cesarz, S., Eisenhauer, N., Martínez-Valderrama, J., Moreno-Jiménez, E., Sala, O., Abedi, M., Ahmadian, N., Alados, C. L., Aramayo, V., Amghar, F., Arredondo, T., Ahumada, R. J., Bahalkeh, K., Ben Salem, F., Blaum, N., Boldgiv, B., Bowker, M. A., Bran, D., Bu, C., Canessa, R., Castillo-Monroy, A. P., Castro, H., Castro, I., Castro-Quezada, P., Chibani, R., Conceição, A. A., Currier, C. M., Darrouzet-Nardi, A., Deák, B., Donoso, D. A., Dougill, A. J., Durán, J., Erdenetsetseg, B., Espinosa, C. I., Fajardo, A., Farzam, M., Ferrante, D., Frank, A. S. K., Fraser, L. H., Gherardi, L. A., Greenville, A. C., Guerra, C. A., Gusmán-Montalvan, E., Hernández-Hernández, R. M., Hölzel, N., Huber-Sannwald, E., Hughes, F. M., Jadán-Maza, O., Jeltsch, F., Jentsch, A., Kaseke, K. F., Köbel, M., Koopman, J. E., Leder, C. V., Linstädter, A., le Roux, P. C., Li, X., Liancourt, P., Liu, J., Louw, M. A., Maggs-Kölling, G., Makhalanyane, T. P., Issa, O. M., Manzaneda, A. J., Marais, E., Mora, J. P., Moreno, G., Munson, S. M., Nunes, A., Oliva, G., Oñatibia, G. R., Peter, G., Pivari, M. O. D., Pueyo, Y., Quiroga, R. E., Rahmanian, S., Reed, S. C., Rey, P. J., Richard, B., Rodríguez, A., Rolo, V., Rubalcaba, J. G., Ruppert, J. C., Salah, A., Schuchardt, M. A., Spann, S., Stavi, I., Stephens, C. R. A., Swemmer, A. M., Teixido, A. L., Thomas, A. D., Throop, H. L., Tielbörger, K., Travers, S., Val, J., Valkó, O., van den Brink, L., Ayuso, S. V., Velbert, F., Wamiti, W., Wang, D., Wang, L., Wardle, G. M., Yahdjian, L., Zaady, E., Zhang, Y., Zhou, X., Singh, B. K., and Gross, N.: Grazing and Ecosystem Service Delivery in Global Drylands, Science, 378, 915–920, https://doi.org/10.1126/science.abq4062, 2022.

Mardia, K. V.: Measures of Multivariate Skewness and Kurtosis with Applications, Biometrika, 57, 519–530, https://doi.org/10.1093/biomet/57.3.519, 1970.

Martin, C., Ménot, G., Thouveny, N., Davtian, N., Andrieu-Ponel, V., Reille, M., and Bard, E.: Impact of Human Activities and Vegetation Changes on the Tetraether Sources in Lake St Front (Massif Central, France), Organic Geochemistry, 135, 38–52, https://doi.org/10.1016/j.orggeochem.2019.06.005, 2019.

Martínez-Sosa, P., Tierney, J. E., Stefanescu, I. C., Crampton-Flood, E. D., Shuman, B. N., and Routson, C.: A Global Bayesian Temperature Calibration for Lacustrine brGDGTs, Geochimica et Cosmochimica Acta, 305, 87–105, https://doi.org/10.1016/j.gca.2021.04.038, 2021.

Martínez-Sosa, P., Tierney, J. E., Pérez-Angel, L. C., Stefanescu, I. C., Guo, J., Kirkels, F., Sepúlveda, J., Peterse, F., Shuman, B. N., and Reyes, A. V.: Development and Application of the Branched and Isoprenoid GDGT Machine Learning Classification Algorithm (BIGMaC) for Paleoenvironmental Reconstruction, Paleoceanography and Paleoclimatology, 38, e2023PA004 611, https://doi.org/10.1029/2023PA004611, 2023.

Moore, D. S., McCabe, G. P., and Craig, B. A.: Introduction to the Practice of Statistics, vol. 4, WH Freeman New York, 2009.

Moreno-Jiménez, E., Plaza, C., Saiz, H., Manzano, R., Flagmeier, M., and Maestre, F. T.: Aridity and Reduced Soil Micronutrient Availability in Global Drylands, Nature Sustainability, 2, 371–377, https://doi.org/10.1038/s41893-019-0262-x, 2019.

Muhammad, S., Müller, T., and Joergensen, R. G.: Relationships between Soil Biological and Other Soil Properties in Saline and Alkaline Arable Soils from the Pakistani Punjab, Journal of Arid Environments, 72, 448–457, https://doi.org/10.1016/j.jaridenv.2007.06.016, 2008.

Naafs, B., Gallego-Sala, A., Inglis, G., and Pancost, R.: Refining the Global Branched Glycerol Dialkyl Glycerol Tetraether (brGDGT) Soil Temperature Calibration, Organic Geochemistry, 106, 48–56, https://doi.org/10/gbjssd, 2017a.

1020 Naafs, B. D. A., Inglis, G. N., Zheng, Y., Amesbury, M. J., Biester, H., Bindler, R., Blewett, J., Burrows, M. A., Del Castillo Torres, D., and Chambers, F. M.: Introducing Global Peat-Specific Temperature and pH Calibrations Based on brGDGT Bacterial Lipids, Geochimica et Cosmochimica Acta, 208, 285–301, https://doi.org/10/f99n9b, 2017b.

Naafs, B. D. A., Oliveira, A. S. F., and Mulholland, A. J.: Molecular Dynamics Simulations Support the Hypothesis That the brGDGT Paleothermometer Is Based on Homeoviscous Adaptation, Geochimica et Cosmochimica Acta, 312, 44–56,
1025 https://doi.org/10.1016/j.gca.2021.07.034, 2021.

Nash, D. J.: World atlas of desertification, vol. 165, Blackwell Publishing Ltd., 1999.

Pérez-Angel, L. C., Sepúlveda, J., Molnar, P., Montes, C., Rajagopalan, B., Snell, K., Gonzalez-Arango, C., and Dildar, N.: Soil and Air Temperature Calibrations Using Branched GDGTs for the Tropical Andes of Colombia: Toward a Pan-Tropical Calibration, Geochemistry, Geophysics, Geosystems, 21, e2020GC008 941, https://doi.org/10.1029/2020GC008941, 2020.

1030 Peterse, F., van der Meer, J., Schouten, S., Weijers, J. W., Fierer, N., Jackson, R. B., Kim, J.-H., and Damsté, J. S. S.: Revised Calibration of the MBT–CBT Paleotemperature Proxy Based on Branched Tetraether Membrane Lipids in Surface Soils, Geochimica et Cosmochimica Acta, 96, 215–229, https://doi.org/10/f4db3v, 2012.

Plaza, C., Zaccone, C., Sawicka, K., Méndez, A. M., Tarquis, A., Gascó, G., Heuvelink, G. B., Schuur, E. A., and Maestre, F. T.: Soil Resources and Element Stocks in Drylands to Face Global Issues, Scientific Reports, 8, 13 788, https://doi.org/10.1038/s41598-018-
1035 32229-0, 2018.

R Core Team: R: A Language and Environment for Statistical Computing, R Foundation for Statistical, Computing. Archives for Scientific Computing, 2020.

Raberg, J. H., Harning, D. J., Crump, S. E., de Wet, G., Blumm, A., Kopf, S., Geirsdóttir, Á., Miller, G. H., and Sepúlveda, J.: Revised Fractional Abundances and Warm-Season Temperatures Substantially Improve brGDGT Calibrations in Lake Sediments, Biogeosciences,
1040 18, 3579–3603, https://doi.org/10.5194/bg-18-3579-2021, 2021.

Raberg, J. H., Flores, E., Crump, S. E., de Wet, G., Dildar, N., Miller, G. H., Geirsdóttir, Á., and Sepúlveda, J.: Intact Polar brGDGTs in Arctic Lake Catchments: Implications for Lipid Sources and Paleoclimate Applications, Journal of Geophysical Research: Biogeosciences, 127, e2022JG006 969, https://doi.org/10.1029/2022JG006969, 2022a.

Raberg, J. H., Miller, G. H., Geirsdóttir, Á., and Sepúlveda, J.: Near-Universal Trends in brGDGT Lipid Distributions in Nature, Science
1045 Advances, 8, eabm7625, https://doi.org/10.1126/sciadv.abm7625, 2022b.

Robles, M., Peyron, O., Brugiapaglia, E., Ménot, G., Dugerdil, L., Ollivier, V., Ansanay-Alex, S., Develle, A.-L., Tozalakyan, P., and Meliksetian, K.: Impact of Climate Changes on Vegetation and Human Societies during the Holocene in the South Caucasus (Vanevan, Armenia): A Multiproxy Approach Including Pollen, NPPs and brGDGTs, Quaternary Science Reviews, 277, 107 297, https://doi.org/10.1016/j.quascirev.2021.107297, 2022.

1050 Rusydi, A. F.: Correlation between Conductivity and Total Dissolved Solid in Various Type of Water: A Review, IOP Conference Series: Earth and Environmental Science, 118, 012 019, https://doi.org/10.1088/1755-1315/118/1/012019, 2018.

Salonen, J. S., Korpela, M., Williams, J. W., and Luoto, M.: Machine-Learning Based Reconstructions of Primary and Secondary Climate Variables from North American and European Fossil Pollen Data, Scientific reports, 9, 1–13, https://doi.org/10/gg978t, 2019.

Sinninghe Damsté, J. S., Ossebaar, J., Abbas, B., Schouten, S., and Verschuren, D.: Fluxes and Distribution of Tetraether Lipids in an Equatorial African Lake: Constraints on the Application of the TEX86 Palaeothermometer and BIT Index in Lacustrine Settings, Geochimica et Cosmochimica Acta, 73, 4232–4249, https://doi.org/10.1016/j.gca.2009.04.022, 2009.

So, R. T., Lowenstein, T. K., Jagniecki, E., Tierney, J. E., and Feakins, S. J.: Holocene Water Balance Variations in Great Salt Lake, Utah: Application of GDGT Indices and the ACE Salinity Proxy, Paleoceanography and Paleoclimatology, p. e2022PA004558, https://doi.org/10.1029/2022PA004558, 2023.

Sun, Q., Chu, G., Liu, M., Xie, M., Li, S., Ling, Y., Wang, X., Shi, L., Jia, G., and Lü, H.: Distributions and Temperature Dependence of Branched Glycerol Dialkyl Glycerol Tetraethers in Recent Lacustrine Sediments from China and Nepal, Journal of Geophysical Research: Biogeosciences, 116, 2011.

Sun, W., Zhao, S., Pei, H., and Yang, H.: The Coupled Evolution of Mid- to Late Holocene Temperature and Moisture in the Southeast Qaidam Basin, Chemical Geology, 528, 119 282, https://doi.org/10.1016/j.chemgeo.2019.119282, 2019.

Thomas, E. K., Clemens, S. C., Sun, Y., Huang, Y., Prell, W., Chen, G., Liu, Z., and Loomis, S.: Midlatitude Land Surface Temperature Impacts the Timing and Structure of Glacial Maxima, Geophysical Research Letters, 44, 984–992, https://doi.org/10.1002/2016gl071882, 2017.

Tierney, J. E., Poulsen, C. J., Montañez, I. P., Bhattacharya, T., Feng, R., Ford, H. L., Hönisch, B., Inglis, G. N., Petersen, S. V., Sagoo, N., Tabor, C. R., Thirumalai, K., Zhu, J., Burls, N. J., Foster, G. L., Goddéris, Y., Huber, B. T., Ivany, L. C., Kirtland Turner, S., Lunt, D. J., McElwain, J. C., Mills, B. J. W., Otto-Bliesner, B. L., Ridgwell, A., and Zhang, Y. G.: Past Climates Inform Our Future, Science, 370, eaay3701, https://doi.org/10.1126/science.aay3701, 2020.

Trabucco, A. and Zomer, R.: Global Aridity Index and Potential Evapo-Transpiration (ET0) Climate Database v2. CGIAR Consortium for Spatial Information (CGIAR-CSI), 2018.

Unkelbach, J., Kashima, K., Punsalpaamuu, G., Shumilovskikh, L., and Behling, H.: Decadal High-Resolution Multi-Proxy Analysis to Reconstruct Natural and Human-Induced Environmental Changes over the Last 1350 Cal. Yr BP in the Altai Tavan Bogd National Park, Western Mongolia, The Holocene, 30, 1016–1028, https://doi.org/10.1177/0959683620908662, 2020.

Véquaud, P., Thibault, A., Derenne, S., Anquetil, C., Collin, S., Contreras, S., Nottingham, A. T., Sabatier, P., Werne, J. P., and Huguet, A.: FROG: A Global Machine-Learning Temperature Calibration for Branched GDGTs in Soils and Peats, Geochimica et Cosmochimica Acta, 318, 468–494, https://doi.org/10.1016/j.gca.2021.12.007, 2022.

Wang, H. and Liu, W.: Soil Temperature and brGDGTs along an Elevation Gradient on the Northeastern Tibetan Plateau: A Test of Soil brGDGTs as a Proxy for Paleoelevation, Chemical Geology, 566, 120 079, https://doi.org/10.1016/j.chemgeo.2021.120079, 2021.

Wang, H., Liu, W., and Lu, H.: Appraisal of Branched Glycerol Dialkyl Glycerol Tetraether-Based Indices for North China, Organic Geochemistry, 98, 118–130, https://doi.org/10.1016/j.orggeochem.2016.05.013, 2016.

Wang, H., An, Z., Lu, H., Zhao, Z., and Liu, W.: Calibrating Bacterial Tetraether Distributions towards in Situ Soil Temperature and Application to a Loess-Paleosol Sequence, Quaternary Science Reviews, 231, 106 172, https://doi.org/10.1016/j.quascirev.2020.106172, 2020.

Wang, H., Liu, W., He, Y., Zhou, A., Zhao, H., Liu, H., Cao, Y., Hu, J., Meng, B., Jiang, J., Kolpakova, M., Krivonogov, S., and Liu, Z.: Salinity-Controlled Isomerization of Lacustrine brGDGTs Impacts the Associated MBT5ME' Terrestrial Temperature Index, Geochimica et Cosmochimica Acta, 305, 33–48, https://doi.org/10.1016/j.gca.2021.05.004, 2021.

Wang, H., Liu, Z., Zhao, H., Cao, Y., Hu, J., Lu, H., Zhao, Z., Cai, Z., Liu, X., and Liu, W.: New Calibration of Terrestrial brGDGT Paleothermometer Deconvolves Distinct Temperature Responses of Two Isomer Sets, Earth and Planetary Science Letters, 626, 118 497, https://doi.org/10.1016/j.epsl.2023.118497, 2024.

Wang, M., Zheng, Z., Zong, Y., Man, M., and Tian, L.: Distributions of Soil Branched Glycerol Dialkyl Glycerol Tetraethers from Different Climate Regions of China, Scientific reports, 9, 1–8, https://doi.org/10.1038/s41598-019-39147-9, 2019.

Weijers, J. W., Schouten, S., van den Donker, J. C., Hopmans, E. C., and Damsté, J. S. S.: Environmental Controls on Bacterial Tetraether Membrane Lipid Distribution in Soils, Geochimica et Cosmochimica Acta, 71, 703–713, https://doi.org/10/c5w8hf, 2007.

Weijers, J. W., Steinmann, P., Hopmans, E. C., Schouten, S., and Damsté, J. S. S.: Bacterial Tetraether Membrane Lipids in Peat and Coal: Testing the MBT–CBT Temperature Proxy for Climate Reconstruction, Organic Geochemistry, 42, 477–486, https://doi.org/10.1016/j.orggeochem.2011.03.013, 2011.

Wickham, H.: Ggplot2: Elegant Graphics for Data Analysis, Springer, 2016.

Williams, W. D.: Salinisation: A Major Threat to Water Resources in the Arid and Semi-arid Regions of the World, Lakes & Reservoirs: Science, Policy and Management for Sustainable Use, 4, 85–91, https://doi.org/10.1046/j.1440-1770.1999.00089.x, 1999.

Yang, H., Pancost, R. D., Dang, X., Zhou, X., Evershed, R. P., Xiao, G., Tang, C., Gao, L., Guo, Z., and Xie, S.: Correlations between Microbial Tetraether Lipids and Environmental Variables in Chinese Soils: Optimizing the Paleo-Reconstructions in Semi-Arid and Arid Regions, Geochimica et Cosmochimica Acta, 126, 49–69, https://doi.org/10/f5n3gh, 2014.

Yang, H., Lü, X., Ding, W., Lei, Y., Dang, X., and Xie, S.: The 6-Methyl Branched Tetraethers Significantly Affect the Performance of the Methylation Index (MBT′) in Soils from an Altitudinal Transect at Mount Shennongjia, Organic Geochemistry, 82, 42–53, https://doi.org/10.1016/j.orggeochem.2015.02.003, 2015.

Zang, J., Lei, Y., and Yang, H.: Distribution of Glycerol Ethers in Turpan Soils: Implications for Use of GDGT-based Proxies in Hot and Dry Regions, Frontiers of Earth Science, 12, 862–876, https://doi.org/10/gfb6xq, 2018.

Zhao, B., Castañeda, I. S., Bradley, R. S., Salacup, J. M., de Wet, G. A., Daniels, W. C., and Schneider, T.: Development of an in Situ Branched GDGT Calibration in Lake 578, Southern Greenland, Organic Geochemistry, 152, 104 168, https://doi.org/10.1016/j.orggeochem.2020.104168, 2021.
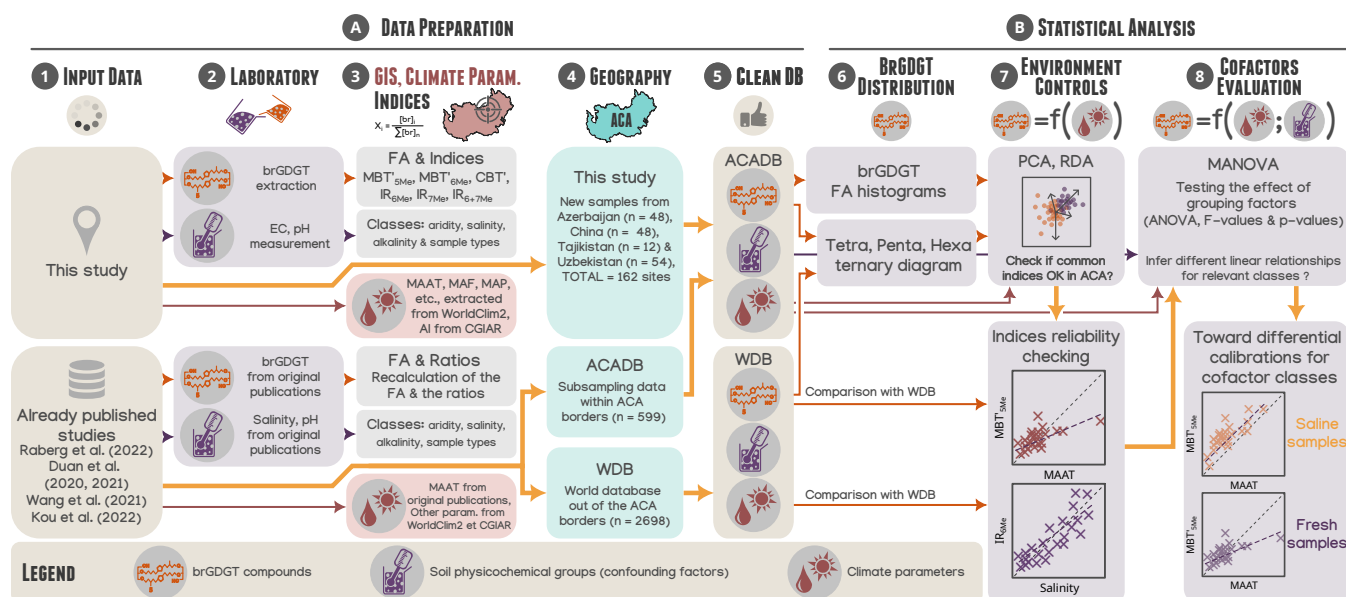
Figure 2. Methodological workflow followed in this study: from the first methodological step (input data – left-hand side) to the final results and perspectives. Each column of boxes represents a methodological step carried out for the data process (**A**) and the statistical analysis (**B**).
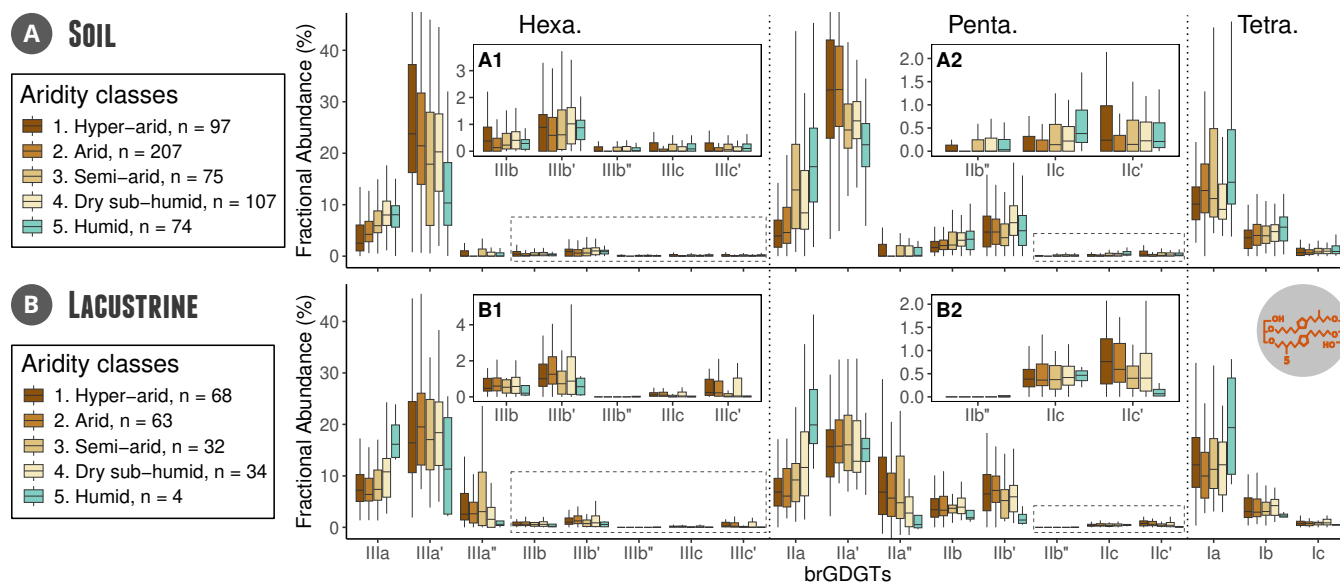
Figure 3. Distribution of individual brGDGTs grouped by aridity index, following the five aridity classes (Nash, 1999) in the ACADB for soil (**A**) and lacustrine samples (**B**). The brGDGT fractional abundances (FA) are displayed with ' for the 6-methyl and '' for the 7-methyl isomers. The hinges of the boxplots show the 25% (Q1) and 75% (Q3) quantiles, the middle horizontal line indicates the median, and the whiskers extend to the most extreme data points that lie within 1.5 × the inter-quartile range (i.e., Q3 - Q1). Points beyond the whiskers are considered outliers and are not shown here. The compounds of lowest abundances (mean value below 5%) are zoomed on panels **A1**, **A2**, **B1** and **B2**.
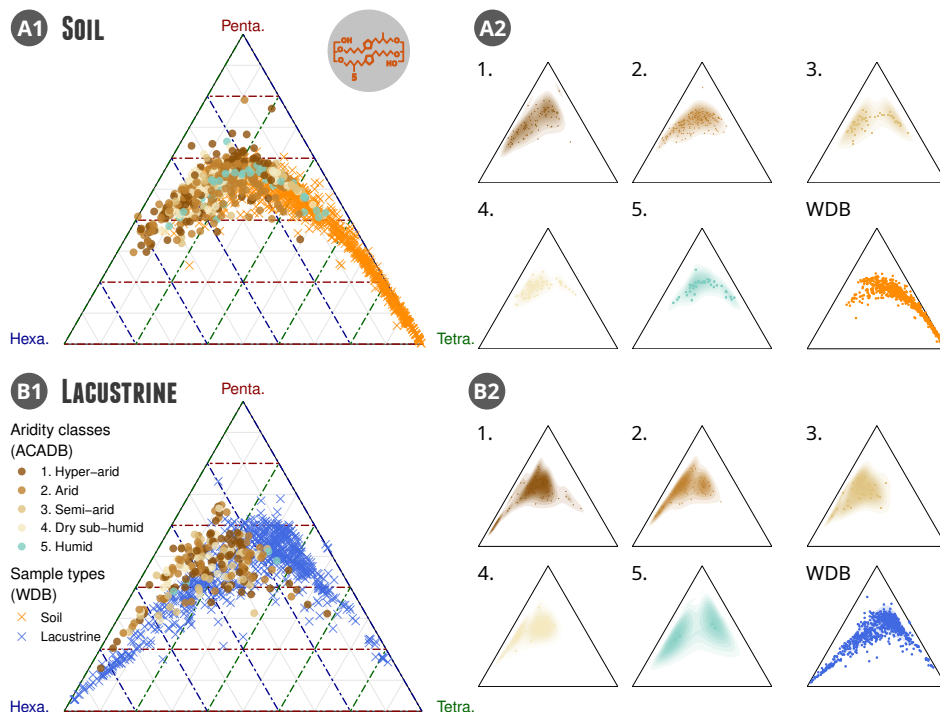
Figure 4. Ternary diagram showing the relative importance of tetra-, penta-, and hexamethylated brGDGT compounds for (**A**) soil samples and (**B**) lacustrine samples. ACADB samples (dots) are compared to WDB ones (crosses). The plots are displayed by aridity classes. Panels **A1** and **B1** overlay the ACADB and WDB, while panels **A2** and **B2** distinctly present the distribution of each aridity class for soils (**A**) and lacustrine samples (**B**).
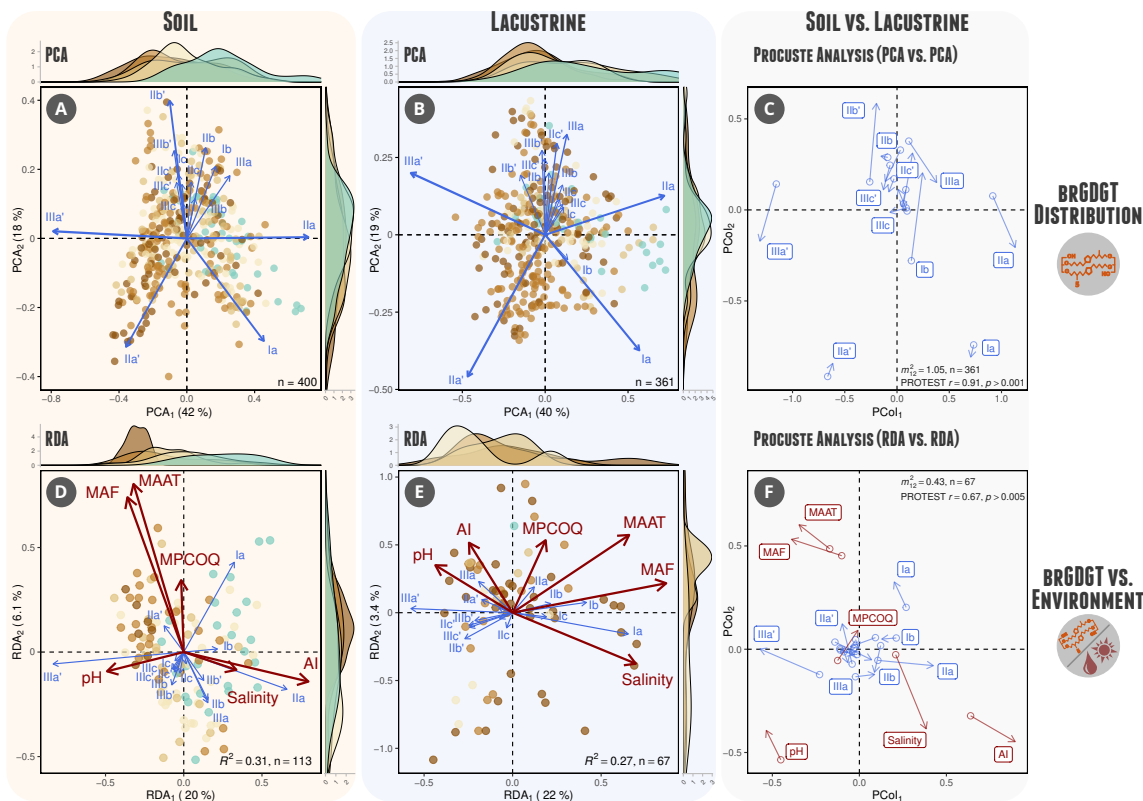
Figure 5. Multivariate analyses of the ACA brGDGT surface samples highlighting the brGDGT distribution using Principal Component Analysis (PCA) for soil (**A**) and lacustrine (**B**) samples, and (**C**) the Procrustes rotation analysis to compare the distribution of the brGDGTs along the loadings of the two PCAs (i.e., multivariate configurations similarity assessment). Then, Redundancy Analyses (RDA) track the main environmental drivers of soil (**D**) and lacustrine (**E**) sample distribution, and the Procrustes rotation analysis compares them (**F**). Analyses were performed only on the 5- and 6-methyl due to the few number of 7-methyl measurements in the database. The most contributing environmental drivers (Aridity Index, salinity, mean air temperature of Months Above Freezing, Mean Annual Air Temperature, Mean Precipitation of the Cold Quarter, pH and Altitude) were selected using a Variance Inflation Factor test (i.e., VIF < 10 for all). The PCA is performed on the whole ACA dataset (n_{soil} = 400 and $n_{lac.}$ = 361), while the RDA only covers 113 soil and 67 lacustrine samples due to scarce pH and salinity measurements available. The colour code for dots corresponds to the five aridity classes.
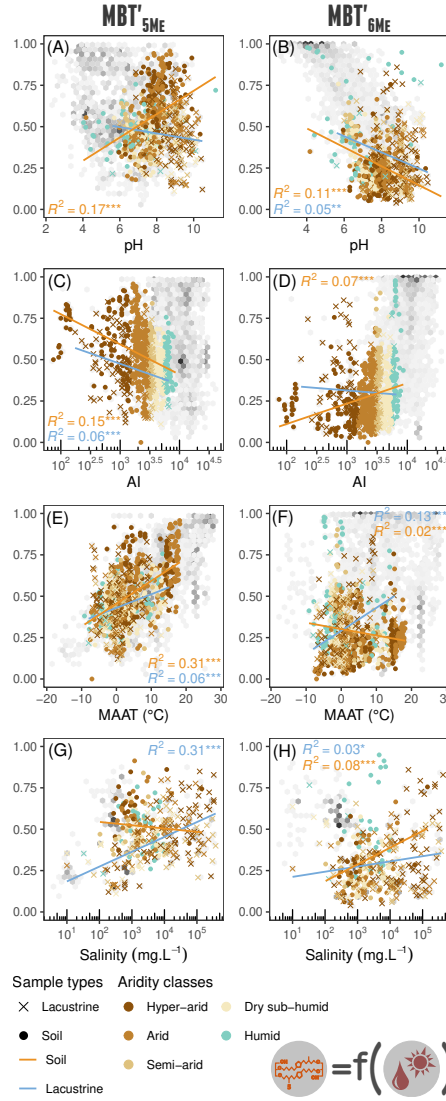
Figure 6. MBT'_{5Me} and MBT'_{6Me} relationships with pH (**A** and **B**), Aridity Index (**C** and **D**), MAAT (**E** and **F**), and salinity (**G** and **H**). The colour refers to the aridity classes for the samples. Two groups per sample type (i.e., lacustrine and soil) are used to infer linear relationships. The grey hexagonal bins show the sample density from the WDB. R^2 values are shown only for statistically significant regressions ($p <$ 0.05), while p-values below 0.001, 0.01, and 0.05 are indicated with ***, **, and *, respectively.
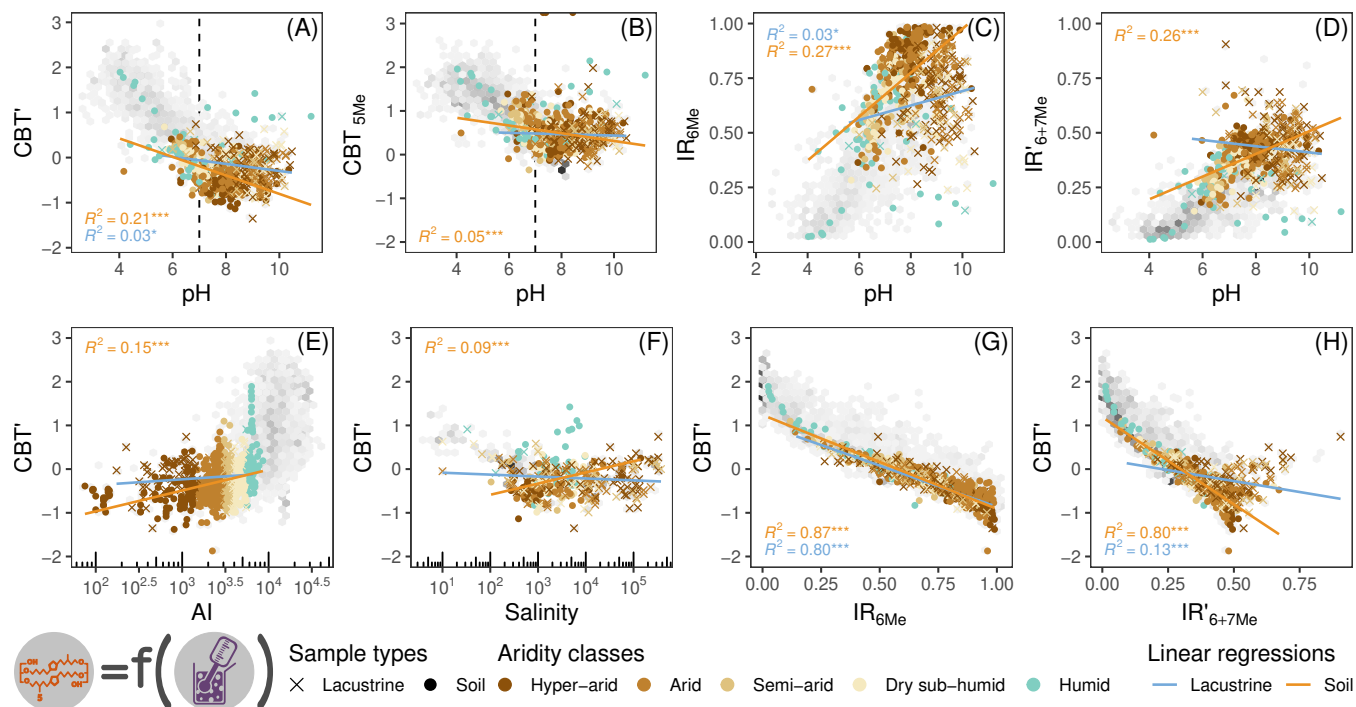
Figure 7. pH-related indices, mainly cyclisation indices (CBT' and ~~CBT'$_{5Me}$~~ CBT$_{5Me}$) and isomer ratios (IR$_{6Me}$ and IR$'_{6+7Me}$) are shown. Linear regressions are tested with pH (**A** to **D**), AI (**E**) and salinity (**F**) and among them (**G** and **D**). The colours refer to the aridity classes for the samples. Two groups by sample type (i.e., lacustrine and soil) are used to infer linear relationships. The grey hexagonal bins show the sample density from the WDB. AI and salinity are displayed on $\log_{10}$ scale. R^2 values are shown only for statistically significant regressions ($p<0.05$), while p-values below 0.001, 0.01, and 0.05 are indicated with ***, **, and *, respectively.
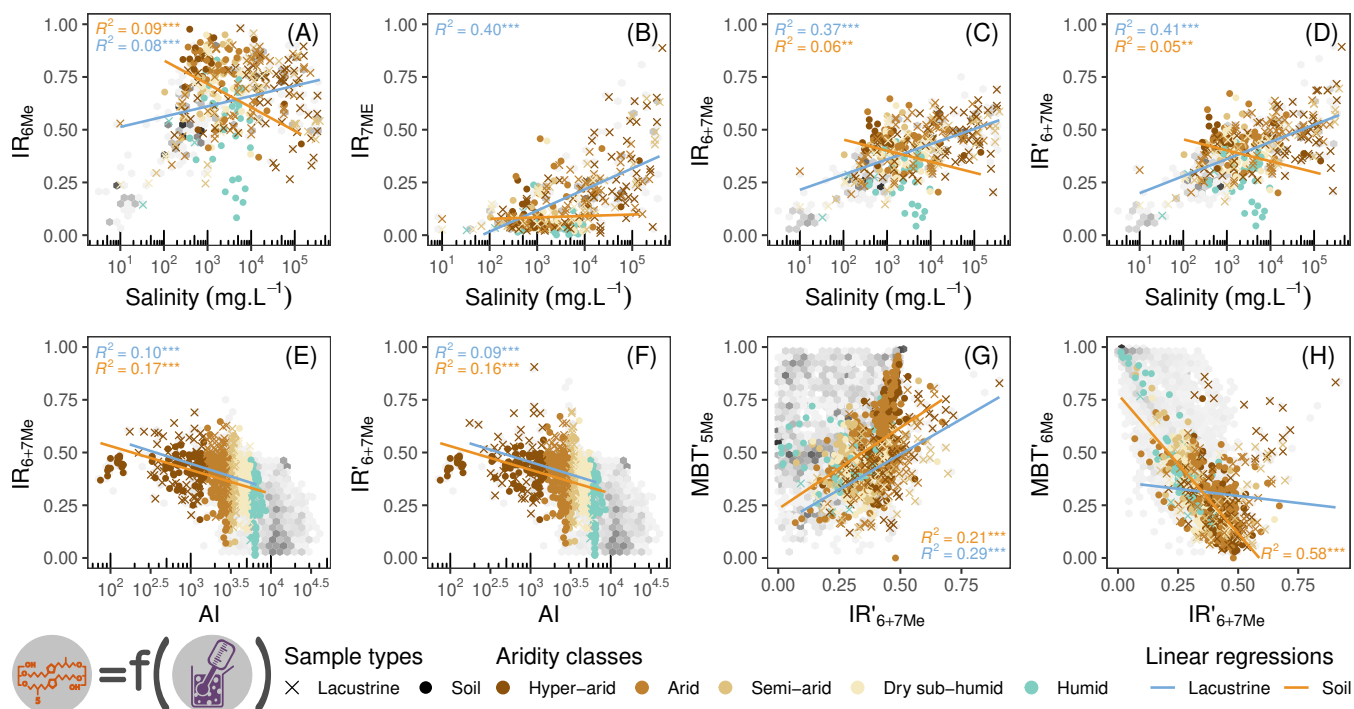
Figure 8. Salinity-related indices: IR_{6Me}, IR_{7Me}, IR_{6+7Me} and IR'_{6+7Me} are the most ubiquitous brGDGT-based indexes used to infer salinity in ACA. The indices are compared to salinity (**A** to **D**), the Aridity Index (**E** and **F**), MBT'_{5Me} and MBT'_{6Me} (**G** and **H**). The colours refer to sample aridity classes. Two groups per sample type (i.e., lacustrine and soil) are used to infer linear relationships. The grey hexagonal bins show the sample density from WDB. AI and salinity are displayed on a $\log_{10}$ scale. R^2 values are shown only for statistically significant regressions ($p<0.05$), while p-values below 0.001, 0.01, and 0.05 are indicated with ***, **, and *, respectively.
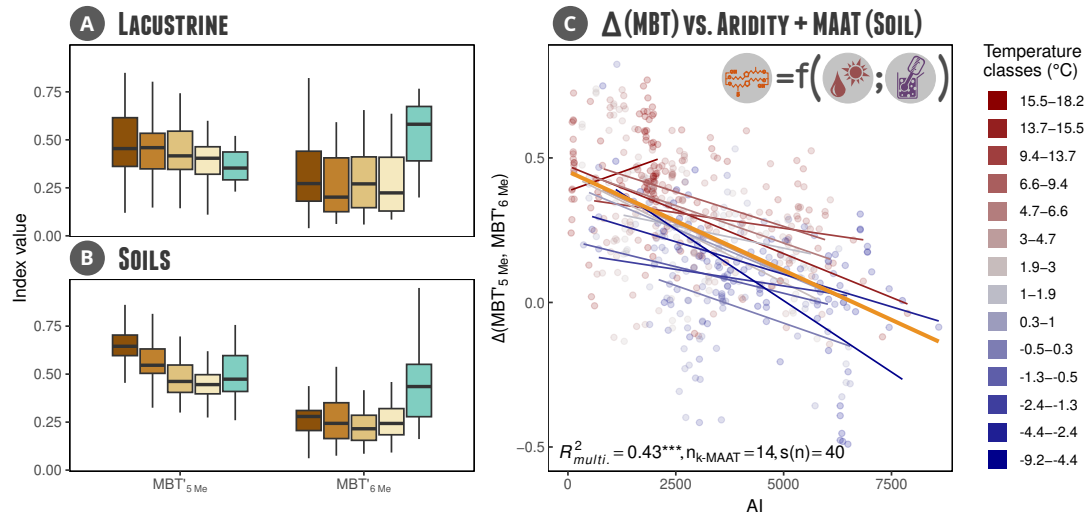
Figure 9. Illustration of the approach comparing $MBT'5Me$ and $MBT'6Me$ to investigate interactions between MAAT, aridity, and sample type. Boxplots of both indices are shown by aridity classes (see Fig.1 for colour codes), separately for soil (**A**) and lacustrine (**B**) samples. Panel **C** displays the relationship between $\Delta(MBT'5Me, MBT'6Me)$ and the Aridity Index for soil samples, across 14 groups of Mean Annual Air Temperature, each containing approximately 40 samples. The orange line indicates the overall regression trend. Corresponding univariate regressions with AI are shown in Fig. S.5.
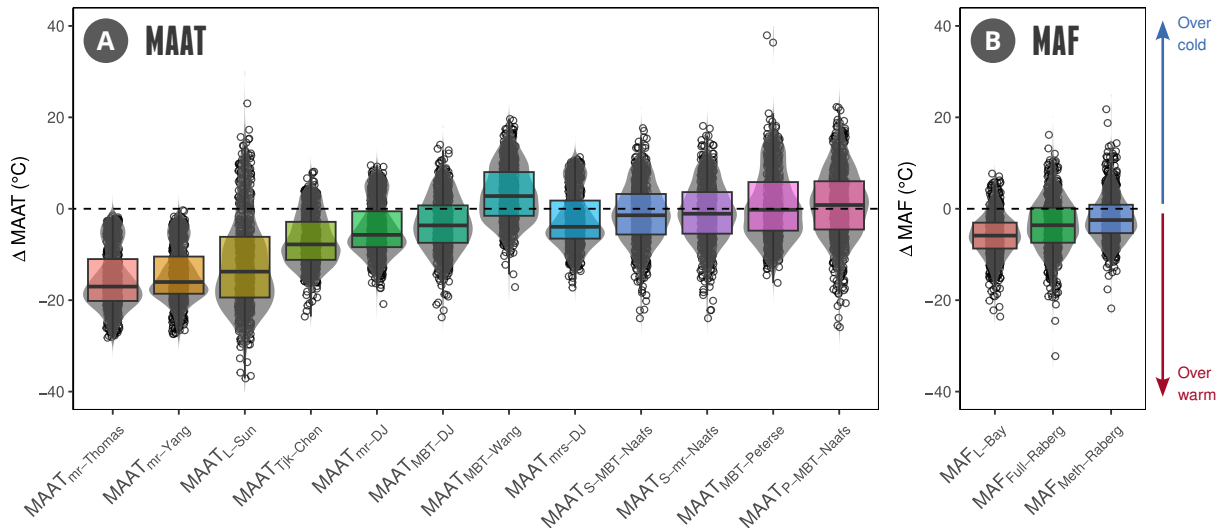
Figure 10. Temperature residuals derived from 15 different brGDGT-temperature calibrations for the Mean Annual Air Temperature (**A**) and the mean air temperature of Months Above Freezing (**B**). The different calibration methods, formulas and RMSE are available in Table S.6. For each calibration original publication, see Sun et al. (2011); Peterse et al. (2012); De Jonge et al. (2014); Yang et al. (2014); Wang et al. (2016); Naafs et al. (2017a, b); Thomas et al. (2017); Chen .
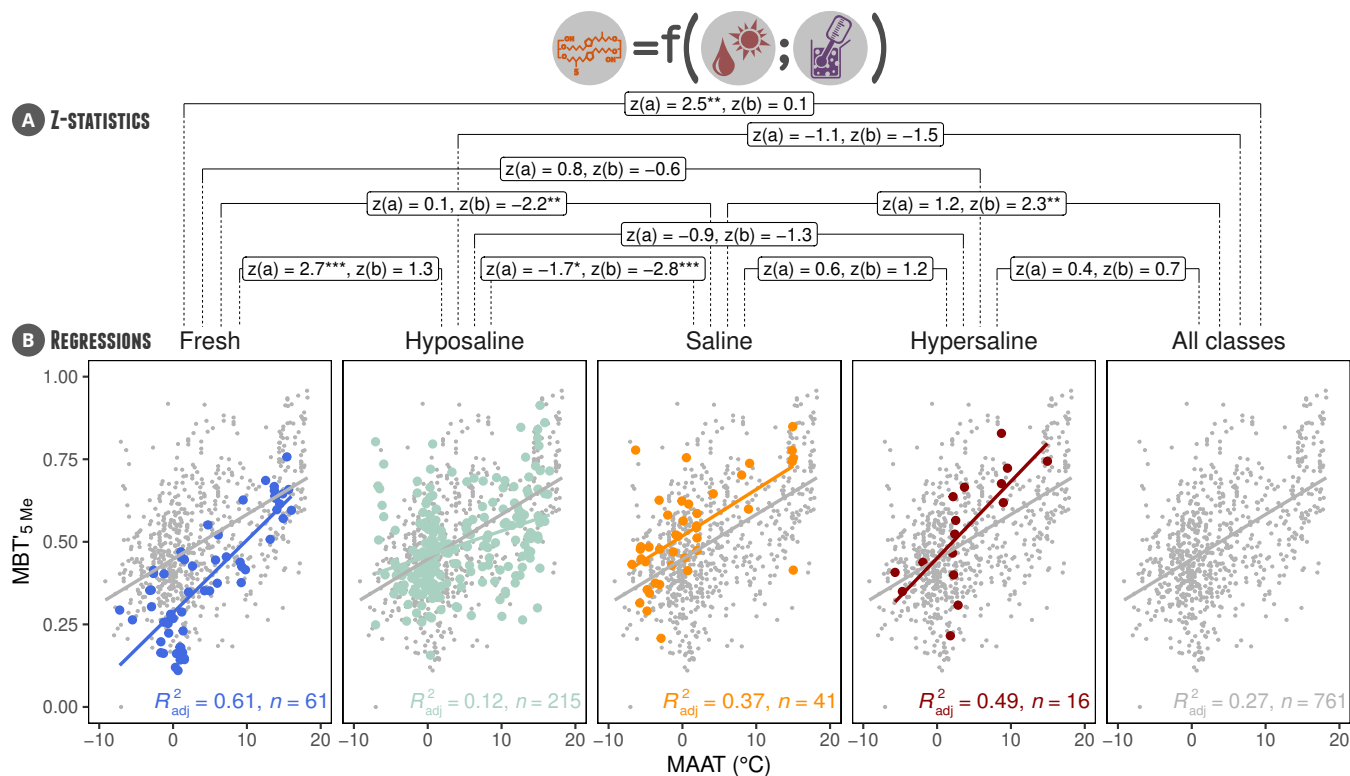
Figure 11. Effect of salinity (i.e., the TDS of each surface sample) on the linear relationship between temperature (here MAAT) and the MBT'_{5Me}. ~~The analysis is based on~~ Panel **A** shows the ~~full ACADB. Based on~~ results of the z-statistic tests assessing significant differences in slopes and intercepts between salinity classes~~(i.e.,~~. Panel **B** presents linear regressions for fresh, hyposaline, saline, and hypersaline ~~)~~classes, ~~different temperature calibrations~~ based on the ~~degree~~ full ACADB. For each salinity group, temperature calibrations ~~of methylation with the form~~ MAAT = a × MBT'_{5Me} + b are proposed (**B**). ~~Using the~~ The z-statistic ~~with its *p*-value~~ method (Clogg et al., 1995) ~~,~~ evaluates the significance of ~~the difference between the slopes~~ slope (a) ~~of the linear regression is evaluated. Similarly, the *z*-statistic was used for the~~ and intercept (b) differences ~~. For~~ across two classes (grey lines link the two classes with their z-statistics on Panel **A**). The p-values ~~we have~~ of the z-statistic are displayed with *** for ~~p~~$p \leq 0.01$, ** for ~~p~~$p \leq 0.05$, and * for ~~p~~$p \leq 0.1$.